A4— 146-32

FINAL REPORT
MATHEMATICAL MODELING OF THE FORMATION AND DYNAMICS OF ACIDIC AEROSOLS

by

Christodoulos Pilinis and John H. Seinfeld

FINAL REPORT

MATHEMATICAL MODELING OF THE FORMATION AND DYNAMICS OF ACIDIC AEROSOLS

by

Environmental Quality Laboratory

California Institute of Technology

Pasadena, Ca 91125

John H. Seinfeld, Principal Investigator

submitted to

State of California Air Resources Board

under

Agreement A4-146-32

October 28, 1987

ABSTRACT

A mathematical model has been developed to predict the chemical composition and size distribution of ambient aerosols containing sulfate, nitrate, ammonium, water, sodium, chloride and organic species. The model has been implemented in a trajectory framework and has been employed to predict the size and composition distributions of aerosol in the South Coast Air Basin on August 31, 1982.

DISCLAIMER

The statement and conclusions in this report are those of the contractor and not necessarily those of the California Air Resources Board. The mention of commercial products, their source or their use in connection with material reported herein is not to be construed as either an actual or implied endorsement of such products.

TABLE OF CONTENTS

CHAPTER 1

SUMMARY AND CONCLUSIONS

SUMMARY AND CONCLUSIONS

Atmospheric aerosol can generally be considered to consist of a mixture of sulfates, nitrates, water, ammonium, elemental and organic carbon and dust. The sulfate component of the aerosol arises from the gas-phase oxidation of SO_2 and from the emission of primary sulfates. Nitrate arises from the gas phase conversion of NO_x to nitric acid followed by reaction with ammonia or other species such as sea salt. The organic portion of the aerosol arises from direct primary particulate carbon emissions or from the gas phase conversion of gaseous organic precursors to condensable organic products.

A major goal of air quality modeling over the past decade or more has been to predict the concentration levels of gaseous primary and secondary pollutants. The next major goal in air quality modeling is to predict the chemical composition and size distribution of the ambient aerosol. Prediction of the concentration levels of gaseous species has required the development of chemical reaction mechanisms capable of describing the gas phase transformations. To predict aerosol sizes and compositions, it is necessary to account not only for the gas phase processes, particularly those that lead to aerosol products, but also the transport of gases to the surfaces of particles, formation of new particles by nucleation, shaping of the size distribution by coagulation, and the equillibration of the particles with the local gaseous environment.

This project presents the first comprehensive urban aerosol model. The model includes all relevant aerosol phenomena, nucleation, condensation, coagulation, chemical equilibria and dry deposition. The essential question approached in this work is- given gas phase concentrations of sulfate, nitrate, ammonium, sodium, chloride, precursor organics, relative humidity and temperature, predict the size and chemical composition distribution of the aerosol.

The particulate nitrate, ammonium, chloride and water concentrations are governed

by thermodynamic considerations whereas the sulfate and organic concentrations are presumed to be governed by primary emissions and by the the rates of gas phase conversion of SO_2 and organic precursors. Using the model developed in this work, we have shown, for the first time how the observed existence of liquid water in the aerosol phase at low relative humidities can be explained by means of thermodynamic equilibrium. The model successfully predicted the amount and composition of the aerosol observed at Long-Beach CA during the episode of Aug. 30-31, 1982. With this work the prospect now exists to interface the aerosol module with a gas phase, grid-based photochemical model to predict simultaneously gaseous and aerosol levels in the atmosphere. Thus, it is now possible to calculate the acidic composition of the gas and aerosol phases and the rates of deposition of both gaseous and particulate acidic species. The model developed in this project is a key element in a comprehensive acid deposition assessment that accounts for both gaseous and particulate acidic species.

CHAPTER 2

MATHEMATICAL MODELING OF THE DYNAMICS OF MULTICOMPONENT ATMOSPHERIC AEROSOLS

MATHEMATICAL MODELING OF THE DYNAMICS OF MULTICOMPONENT ATMOSPHERIC AEROSOLS

Christodoulos Pilinis and John H. Seinfeld*

Department of Chemical Engineering

California Institute of Technology

Pasadena, CA 91125

and

Christian Seigneur+

Systems Applications, Inc.

101 Lucas Valley Road

San Rafael, CA 94903

ABSTRACT

A model is developed to simulate the dynamics of multicomponent atmospheric aerosols, including new particle formation by homogeneous heteromolecular nucleation, gas-to-particle conversion, coagulation, and dry deposition. Both equilibrium and non-equilibrium aspects involving sulfate, nitrate, and ammonium compounds are considered. The model is used to predict the dynamics of the composition of the aerosol observed on an air trajectory in the Los Angeles basin on August 31, 1982.

* To whom correspondence should be addressed.

+ Present address: Bechtel National, Inc., Environmental Sciences Department, 50 Beale Street, P.O. Box 3965, San Francisco, California 94119.

Indexing Key Words

Aerosols, Mathematical model.

INTRODUCTION

Atmospheric aerosols are, in general, multicomponent particles with sizes ranging roughly from 0.01 to 10 μm diameter. These particles evolve as a result of gas-to-particle conversion and coagulation, are augmented through the formation of fresh particles by nucleation and through the continuous introduction of primary particles, and are removed by wet and dry deposition.

To predict how atmospheric aerosol levels depend on gaseous and particulate source emissions, and specifically how such levels might be expected to vary given changes in primary emissions, requires the development of aerosol air quality models. Whereas the development, evaluation and use of gas-phase air quality models has received considerable attention, there has not been available an air quality model capable of simulating the dynamics of multicomponent atmospheric aerosols that includes new particle formation by nucleation, growth or evaporation due to gas-to-particle or particle-to-gas conversion, and coagulation. The object of the present work is to present the first urban multicomponent aerosol model and to illustrate its application to the Los Angeles basin.

A considerable body of work has preceded the model we will present and it is useful to review that work briefly to provide the context within which the current model lies.

A spatially-uniform, dynamic multicomponent aerosol can be characterized by its size-composition distribution function $n(m,t)$, where $m = (m_1, m_2, ..., m_k)^T$, such that $n(m,t)dm$ is the number of particles per volume of gas with mass composition in the range $[m_1, m_1+dm_1]$, $[m_2, m_2+dm_2]$, etc.(Specification of the complete chemical composition of a particle in principle specifies the particle's size.) For an aerosol that can be completely characterized by its size , e.g. one comprised of a single chemical component, its size distribution function is just $n(D_p,t)$, where $n(D_p,t)dD_p$ is the number of particles per volume of gas with diameters in the range $[D_p, D_p + dD_p]$ .The dynamic behavior of n is

governed by the so called general dynamic equation (Gelbard and Seinfeld 1979; Seinfeld 1986). The numerical solution of the general dynamic equation serves as the central core of a model simulating the evolution of aerosols. Significant work has been carried out on techniques for the numerical solution of the general dynamic equation, largely devoted to its form for $n(D_p,t)$ (Gelbard and Seinfeld 1978; Middleton and Brock 1976; Tsang and Brock 1983) Recently several of these approaches have been reviewed and compared (Seigneur et al 1986). Some previous work does exist on the numerical simulation of single-component atmospheric aerosols through solution for $n(D_p,t)$ (Bassett et al 1981; Eltgroth and Hobbs 1979; Middleton and Kiang 1978; Seigneur 1982; Suck and Brock 1979; Tsang and Brock 1982).

An approximate composition of the Los Angeles aerosol is 20% sulfates, 25% nitrates, 10% elemental carbon, 20% organic carbon (primary and secondary), 25% soil, metals and water. The following picture is considered to represent the evolution of such a "typical" particle. Say that a primary carbonaceous particle is emitted and advected from its source by the wind. In the gas-phase, photochemical reactions are occurring converting NO_x to nitric acid (HNO_3), SO_2 to sulfuric acid (H_2SO_4), and reactive organic gases to low vapor pressure condensable species. Water vapor is ubiquitous, and ammonia (NH_3) may also be present in the gas phase. Gas-to-particle conversion of sulfate, nitrate, ammonium and organics occurs as these gas-phase reactions proceed, with the composition of the aerosol continuously adjusting to maintain equilibrium at the local relative humidity and temperature. At high relative humidity the aerosol consists of an aqueous solution of sulfate, nitrate and ammonium ions, while at low relative humidity the resulting aerosol may be completely dry. In the latter case the solid phase is an external mixture of four simple salts, NH_4HSO_4, $(NH_4)_3H(SO_4)_2$, $(NH_4)_2SO_4$ and NH_4NO_3, as well as two mixed salts, $(NH_4)_2SO_4 \bullet 2NH_4NO_3$ and $(NH_4)_2SO_4 \bullet 3NH_4NO_3$ (Stelson and Seinfeld 1982c;

Harrison and Sturges 1984). It is this overall process that we seek to simulate.

We begin with a brief summary of the calculation of aerosol thermodynamic equilibria, followed by a discussion of the simulation of multicomponent aerosol dynamics. The remainder of the paper is devoted to a detailed application of the model developed to simulate the evolution of aerosol along a particular air trajectory in the Los Angeles basin on August 31, 1982.

AEROSOL THERMODYNAMIC EQUILIBRIUM

When the multicomponent nature of the aerosol is considered, one must account for the individual rates of transfer of the various species between the gas and particulate phases. If the sticking coefficient is equal to one then the characteristic time for gas-particle transport for certain species is short enough that chemical equilibrium is established on a time scale much shorter than that over which other changes are taking place. This situation is in fact estimated to be the case for species such as water and ammonium nitrate(Hildelmann et al 1984; Tanner 1983; Russell et al 1983; Russell and Cass 1984). Consequently, chemical equilibrium can be assumed to be instantaneously established for such species. Considerable effort has been devoted to developing the capability to predict the equilibrium chemical composition and physical state of atmospheric sulfate, nitrate, and ammonium aerosols (Bassett and Seinfeld 1983, 1984; Saxena et al 1986; Stelson et al 1979; Stelson and Seinfeld 1982 a, b, c). As noted above, to simulate the evolution of an atmospheric aerosol containing water, sulfates, nitrates, and ammonium it will be necessary to merge the thermodynamic equilibrium calculation into the dynamic solution of the multicomponent general dynamic equation.

From the point of view of numerical simulation we can divide the aerosol evolution into a short time step of non-equilibrium gas-to-particle conversion and coagulation, followed by an instantaneous relaxation to equilibrium. Then more gas-to-particle conversion and

coagulation occur over the next time step, followed again by adjustment of the particle composition (and size) to equilibrium. Thus the structure of the numerical solution will consist of successive steps of non-equilibrium transport and coagulation followed by the reestablishment of gas and particulate phase chemical equilibrium.

Sulfate is produced in the gas phase, by oxidation of SO_2 (Middleton et al 1980), and it is transferred to the particulate phase by either condensation on already existing particles or nucleation. Because of the relatively low vapor pressure of sulfuric acid, the gas-to-particle conversion process can be assumed to be irreversible. In addition, sulfate may be formed through oxidation of SO_2 on the surface of soot aerosol or in aqueous aerosols.

Volatile compounds, such as ammonia, nitric acid, and water, on the other hand, are distributed between the gas and aerosol phases as determined by thermodynamic equilibrium. The distribution by particle size of non-volatile species, such as sulfate, serves as a "core" upon which the distribution of volatile species can be determined.

In considering the equilibrium in the sulfate, nitrate, ammonium system the following components are possible(Bassett and Seinfeld 1983, 1984; Harrison and Sturges 1984; Saxena et al 1986):

gas phase	NH_3, H_2O, HNO_3
liquid phase	NH_4^+, H^+, HSO_4^-, SO_4^{2-}, NO_3^-, H_2O
solid phase	NH_4HSO_4, $(NH_4)_3H(SO_4)_2$, $(NH_4)_2SO_4$, NH_4NO_3
	$(NH_4)_2SO_4 \bullet 2NH_4NO_3$, $(NH_4)_2SO_4 \bullet 3NH_4NO_3$

Three methods have been developed to determine the thermodynamic equilibrium in this system and the computer codes that have resulted are summarized in Table 1. The basic idea of each method is, given the sulfate, nitric acid, and ammonia concentrations, as well as relative humidity and temperature, to determine the equilibrium phases and their

composition by minimizing the total Gibbs free energy of the system, i.e.

$$\min_{n_i} G_{total}$$

subject to

a) conservation of mass

b) $n_i \geq 0$ for all i

AEROSOL DYNAMICS

A spatially homogeneous aerosol undergoing nucleation, condensation and coagulation is simulated by numerical solution of the general dynamic equation. A particularly powerful technique for solving the multicomponent general dynamic equation is the so- called sectional method(Gelbard and Seinfeld 1980; Gelbard et al 1980; Gelbard 1984; Warren and Seinfeld 1985).

The sectional representation of an aerosol distribution approximates the continuous size distribution function with a series of step functions. The particle size may be represented by x, the natural logarithm of the mass of a particle. If one defines $q(x)$ as the continuous aerosol mass distribution function, i.e. $q(x)dx$ is the mass corresponding to particles with logarithm of mass in the range $[x, x + dx]$, then the total mass within each section is given by

$$Q^l = \int_{x_l}^{x_{l+1}} q(x)\, dx \qquad l = 1, 2, \cdots \qquad [1]$$

where x_l, x_{l+1} are the lower and upper bounds of section l, respectively. One assumes that the mass is uniformly distributed within each section.Thus,

$$\overline{q}_l(x) = \frac{Q^l}{x_{l+1} - x_l} \qquad l = 1, 2, \cdots \qquad [2]$$

The number of particles in each section is linearly related to the total aerosol mass within the section , specifically

$$N^l = Q^l \frac{e^{-x_l} - e^{-x_{l+1}}}{x_{l+1} - x_l} \quad [3]$$

Thus the sectional general dynamic equation that describes the evolution of the concentration of species i in the l^{th} section, Q_i^l, takes the following form

$$\frac{\partial Q_i^l}{\partial t} = \left[\frac{\partial Q_i^l}{\partial t}\right]_{cond./evap.} + \left[\frac{\partial Q_i^l}{\partial t}\right]_{coag.} + \left[\frac{\partial Q_i^l}{\partial t}\right]_{sources/sinks} \quad [4]$$

where the first term on the right hand side represents growth due to condensation or shrinkage due to evaporation, the second term represents coagulation and the third term represents sources of new particles through nucleation and primary emissions and removal through wet and dry deposition.

Multicomponent condensation/evaporation

The flux of vapor molecules of species i onto an aerosol particle of diameter d_p, F_i in the case that gas-phase diffusion is the rate determining step, can be described by the Fuchs-Sutugin formula (Fuchs and Sutugin 1971)

$$F_i = 2\pi d_p \mathbf{D_i} \frac{(p_i - p_{di}) f_o(Kn)}{kT} \quad [5]$$

with

$$f_o(Kn) = \frac{1 + Kn}{1 + 1.71Kn + 1.33Kn^2} \quad [6]$$

where Kn is the Knudsen number, $\mathbf{D_i}$ is the diffusion coefficient of species i in the gas phase and $(p_i - p_{di})$ is the difference between the partial pressure of species i in the bulk phase and that at the particle surface. The rate of change of the mass of species i in particles of diameter d_p due to the flux F_i is

$$\frac{dM_i}{dt} = H_i M_{tot} \quad [7]$$

where

$$H_i = \frac{12 D_i (p_i - p_{di}) f_o(Kn) m_{1i}}{\rho_l d_p^2 kT} \qquad [8]$$

and where M_{tot} is the total aerosol mass at time t, ρ_l is the the species density as a liquid or a solid, and m_{1i} is the molecular mass of species i. An assumption associated with Eq.[7] is that ρ_l remains constant as a function of time.

When the aerosol mass distribution has been represented by sections, the growth rate of the mass of component i in section l,

$$\overline{H}_i^l = \frac{\int_{x_l}^{x_{l+1}} q(x) H_i \, dx}{\int_{x_l}^{x_{l+1}} q(x) \, dx} \qquad [9]$$

from Eq.[2] becomes

$$\overline{H}_i^l = \frac{\int_{x_l}^{x_{l+1}} H_i \, dx}{x_{l+1} - x_l} \qquad [10]$$

Therefore, $\overline{H}_i^l Q^l$ is the rate of change of the mass of species i on particles in section l. This growth causes some of the largest particles of the section to migrate into the $(l+1)^{th}$ section while, at the same time, some of the largest particles in the $(l-1)^{th}$ section grow into section l. Exactly the reverse behavior takes place in the case of evaporation. To account for this phenomenon the intersectional condensation rate, $\overline{I}_i^{l+1}$, is defined, such that $\overline{I}_i^{l+1} \, dt$ is the mass of species i that goes from section l to section $l+1$ in the time interval $[t, t+dt]$. As a result the net rate of change of the mass of species i, in section l is given by

$$\left[\frac{dQ_i^l}{dt}\right]_{condensation} = \overline{H}_i^l Q^l - \overline{I}_i^{l+1} + \overline{I}_i^l \qquad [11]$$

Particle number conservation for an aerosol undergoing condensational growth can be used to set the rates of the intersectional condensation (Warren and Seinfeld 1985). The overall intersectional mass flux from the l^{th} section, defined as $\overline{I}^{l+1} = \sum_i \overline{I}_i^{l+1}$, is given by

$$\overline{I}^{l+1} = \frac{\sum_i \overline{H}_i^l Q^l}{1 - e^{-(x_{l+2} - x_l)/2}} \qquad [12]$$

in the case of condensation,and

$$\overline{I}^{l+1} = \frac{\sum_i \overline{H}_i^{l+1} Q^{l+1}}{1 - e^{(x_{l+2} - x_l)/2}} \qquad [13]$$

in the case of evaporation.

The intersectional condensation rate of species i is proportional to the overall intersectional mass flux and it is also proportional to the mass fraction of species i in the l^{th} and $(l+1)^{th}$ sections for condensation and evaporation, respectively, i.e.

$$\overline{I}_i^{l+1} = \frac{Q_i^l}{Q^l} \overline{I}^{l+1} \qquad [14]$$

for condensation, and

$$\overline{I}_i^{l+1} = \frac{Q_i^{l+1}}{Q^{l+1}} \overline{I}^{l+1} \qquad [15]$$

for evaporation. Substitution of [12] and [13] into [14] and [15], respectively, gives

$$\overline{I}_i^{l+1} = \frac{Q_i^l \sum_i \overline{H}_i^l}{1 - e^{-(x_{l+2} - x_l)/2}} \qquad [16]$$

for the case of condensation, and

$$\overline{I}_i^{l+1} = \frac{Q_i^{l+1} \sum_i \overline{H}_i^{l+1}}{1 - e^{(x_{l+2} - x_l)/2}} \qquad [17]$$

for the case of evaporation.

Note that the largest section must be specified large enough so that no particles can grow out of it. Also, the lower bound of the first section must be larger than the size of the critical nucleus for homogeneous nucleation, so that freshly nucleated particles grow into the first section. It is assumed here that the rate of growth of aerosols into the lowest size section is equal to the rate of nucleation of fresh aerosols.

One difficulty that arises when applying the sectional method to atmospheric aerosols is dealing with those species the mass of which in the aerosol phase is thermodynamically

controlled. We need to estimate the intersectional coefficients of the nonvolatiles due to condensation or evaporation of the equilibrium species, the volatiles. Let $Q(t)$ be the overall aerosol mass at time t, i.e $Q(t) = \sum_l Q^l(t)$. Then, one can define a time average rate of aerosol change due to condensation or evaporation of the volatiles, $\overline{H}_v$, so that equation [7] is satisfied, i.e

$$\frac{dQ}{dt} = \overline{H}_v Q \qquad [18]$$

subject to $Q(t_o) = Q_o$. Eq.[18] gives

$$\overline{H}_v = \frac{1}{\Delta t} \ln\left[\frac{Q(t_o + \Delta t)}{Q_o}\right] \qquad [19]$$

where $Q(t_0 + \Delta t)$ is the sum of the nonvolatile species mass, obtained from the non-equilibrium computation, and the volatile species mass, found from the equilibrium portion of the computation, at time $(t_0 + \Delta t)$.

The distribution of the volatiles between sections depends, in general, on the particle size in each section, because the tendency for molecules to escape a small drop into the vapor phase will depend on the size of the drop. If, though, one neglects the effect of surface curvature on vapor pressure, the Kelvin effect, an assumption reasonable for particles for which $d_p \geq 0.01\,\mu$m, the mass of volatiles that condenses in one section is proportional to the mass fraction of the total nonvolatiles in that section. As a result, the intrasectional time average rate of aerosol mass change in the l^{th} section, due to condensation or evaporation of volatile species, is given by

$$\overline{H}_v^l = \frac{1}{\Delta t} \frac{Q_{nv}^l}{Q_{nv}} \ln\left[\frac{Q(t_o + \Delta t)}{Q_o}\right] \qquad [20]$$

where Q_{nv}^l is the mass of the nonvolatiles in the l^{th} section, and Q_{nv} is the total nonvolatile mass in the aerosol phase.

Given $\overline{H}_v^l$ Eqs. [16] and [17] can be used to determine the intersectional rates.

Coagulation

Assuming that only binary collisions occur, the coagulation part of Eq.[4] has the form

$$\frac{dQ^l}{dt} = \sum_{n=1}^{l-1} \beta^a_{n,l-1}\, Q^l\, Q^n - \sum_{n=1}^{L} \beta^b_{n,l}\, Q^l\, Q^n \qquad [21]$$

where $\beta^a_{n,l-1}$ and $\beta^b_{n,l}$ are the sectional coagulation coefficients depending on the total masses of the coagulating particles and L is the total number of sections. (Gelbard and Seinfeld 1980; Gelbard et al 1980; Gelbard 1984). These coagulation calculations are simplified if a geometric constraint for the sectional boundaries is imposed, namely $x_{l+1} - x_l \geq \ln 2$

Homogeneous heteromolecular nucleation

New particles may form by homogeneous nucleation. In the system we are considering nucleation may be either homomolecular or heteromolecular. The candidates for nucleation are H_2SO_4, HNO_3 and secondary organics formed from the atmospheric conversion of hydrocarbons.

Under atmospheric conditions, H_2SO_4 and HNO_3 heteromolecular nucleation with H_2O occurs at a rate many orders of magnitude above that of homogeneous homomolecular nucleation, because heteromolecular nucleation can take place when a mixture of vapors is undersaturated with respect to the pure vapors, as long as it is supersaturated with respect to the critical solution (Middleton and Kiang 1978; Mirabel and Katz 1974; Yue and Hamill 1979).

Since $H_2SO_4 - H_2O$ nucleates at 6 to 8 orders of magnitude lower concentration than does nitric acid at the same relative humidity, we account only for homogeneous heteromolecular nucleation of sulfuric acid with water here. For the present study we neglect any nucleation that might be occurring involving secondary organics.

The classical rate of binary nucleation of $H_2SO_4 - H_2O$ when the vapor number concentration of water is much larger than that of sulfuric acid is given by (Middleton and Kiang 1978; Mirabel and Katz 1974; Yue and Hamill 1979).

$$J = 4\pi r^{*2} \frac{p_{H_2SO_4}}{(2\pi m_{H_2SO_4} kT)^{1/2}} exp\left[-\frac{\Delta G^*}{kT}\right] \qquad [22]$$

where r^* and ΔG^* are the critical cluster radius and free energy, respectively, and where $p_{H_2SO_4}$ and $m_{H_2SO_4}$ are the partial pressure and molecule mass of sulfuric acid respectively.

To calculate J from Eq.[22] one needs to know the quantities ΔG^* and r^*. The free energy of formation of a cluster containing n_1 and n_2 molecules of H_2SO_4 and H_2O, respectively, is given by

$$\Delta G = n_1(\mu_{1l} - \mu_{1g}) + n_2(\mu_{2l} - \mu_{2g}) + 4\pi r^2 \gamma \qquad [23]$$

where μ_{1l}, μ_{2l}, μ_{1g}, μ_{2g} are the chemical potentials of the two components in the liquid and gas phase, respectively, for a macroscopic amount of liquid, and γ is the surface tension.

To find the Gibbs free energy, the radius, and the composition of the critical cluster one has to solve Eq.[23] together with the saddle point conditions (Middleton and Kiang 1978; Mirabel and Katz 1974; Yue and Hamill 1979).

$$\frac{\partial \Delta G}{\partial n_1}\Big)_{n_2} = \mu_{1l} - \mu_{1g} + \frac{2\gamma V_1}{r^*} - \frac{3X^*V}{r^*}\frac{d\gamma}{dX}\Big)_{X=X^*} = 0 \qquad [24]$$

$$\frac{\partial \Delta G}{\partial n_2}\Big)_{n_1} = \mu_{2l} - \mu_{2g} + \frac{2\gamma V_2}{r^*} + \frac{3(1-X^*)V}{r^*}\frac{d\gamma}{dX}\Big)_{X=X^*} = 0 \qquad [25]$$

$$X = \frac{n_2}{n_1 + n_2} \qquad [26]$$

$$\frac{4}{3}\pi r^{*3} = (n_1^* + n_2^*)V \qquad [27]$$

where V_1 and V_2 are the partial molar volumes, and V is the molar volume of the binary solution, at critical composition.

The location of the saddle point is obtained by solving the system of equations [23]-[27] numerically, using Newton's method. Since in the atmosphere the gas densities of sulfuric acid and water are very low, the ideal gas law can be used to obtain the terms $\mu_{ig} - \mu_{il}$ appearing in Eqs.[24]and [25]. Molar volumes have been calculated from the data on density and composition given in Perry (Perry and Chilton 1973). Calculated values were then fitted by a fifth degree polynomial. Partial molar volumes were determined by calculating the intercepts of the tangent to the polynomial with the axes. Vapor pressure data for aqueous sulfuric acid have been taken from the work of Gmitro and Vermeulen (1964) and were fitted with a logarithmic function. Surface tensions for the mixture of sulfuric acid and water were obtained from the data of Sabinina and Terpugow (1935) and have been fitted by a fifth degree polynomial.

TRAJECTORY AEROSOL MODEL

A form commonly used for air quality models is the Lagrangian trajectory model used to simulate the changes occurring in a hypothetical air parcel advected by the mean wind field(Liu and Seinfeld 1975; Tilden and Seinfeld 1982). The model is particularly useful in providing a means to examine the sensitivity of air quality to changes in key variables without incurring the computational requirements of a three-dimensional grid model. As applied to the aerosol model, the governing equations for Q_i^l are

$$\frac{\partial Q_i^l}{\partial t} = \frac{\partial}{\partial z}\left(K_{zz}\frac{\partial Q_i^l}{\partial z}\right) + \left[\frac{\partial Q_i^l}{\partial t}\right]_{growth/shrinkage} + \left[\frac{\partial Q_i^l}{\partial t}\right]_{coagulation} - \left[\frac{\partial Q_i^l}{\partial t}\right]_{deposition} + S_i^l(x,y,z,t) \qquad [28]$$

with initial conditions

$$Q_i^l(x,y,z,0) = Q_{i0}^l(x,y,z) \qquad [29]$$

and boundary conditions

$$K_{zz}\frac{\partial Q_i^l}{\partial z} = 0 \qquad for \qquad z = H \qquad [30]$$

$$E_i^l + K_{zz}\frac{\partial Q_i^l}{\partial z} - v_{gi}Q_i^l = 0 \qquad for \qquad z = 0 \qquad [31]$$

where $K_{zz}(z)$ is the eddy vertical diffusion coefficient, H is the height of the vertical column, E_i^l is the emission flux per unit area of species i in the l^{th} section, v_{gi} is the deposition velocity, and $S_i^l(x,y,z,t)$ is the rate of increase of species i in the l^{th} section due to nucleation or direct injection of aerosol into the atmosphere.

Given the emission inventory, meteorological conditions and concentrations of all the gaseous pollutants at time t, the trajectory model calculates the concentrations of the various gases at time $t+\Delta t$, as well as the evolution of Q_i^l in the aerosol phase due to eddy diffusion and deposition. Then the non-equilibrium portion of the aerosol model is used to update the sulfate distribution in the aerosol phase through the condensation, coagulation, and nucleation portions of the general dynamic equation. Subsequently the equilibrium solution is used to calculate the total aerosol mass and chemical composition, as well as to update the size distribution of the aerosol, by calculating the intersectional movement of particles, due to reestablishment of the equilibrium of the volatile species. The resulting aerosol size and chemical composition distribution at time $t + \Delta t$ is used as input for the subsequent step.

The initial size and chemical composition distribution of the aerosol is required. Since the rates of generation of various condensable organics are not yet well established, we neglect here the organic contribution to gas-to-particle conversion, although the model has the ability to include organics as data become available. For convenience the initial sulfate distribution is assumed to be log-normal. At the prevailing gas-phase conditions at the beginning of the trajectory the volatiles are assumed to be distributed between the gaseous

and the aerosol phase so that equilibrium is achieved.

A compromise between reasonable accuracy and computational cost is obtained by assuming that the aerosol size distribution is described by nine sections in the range between 0.01 and 20 μm, while the air parcel is divided into ten equally spaced vertical grids.

The vertical diffusion coefficient depends on atmospheric stability and height. The gas-phase chemical kinetics are simulated using the reaction mechanism presented by Russell et al (1983). Dry deposition of aerosols is calculated on the basis of a single, size-independent deposition velocity v_g (Russell et al 1983). Nitrate aerosol results from the formation of nitric acid vapor by a variety of paths, including reaction of NO_2 with hydroxyl radical. Formation of sulfuric acid takes place through the gas-phase oxidation of SO_2:

$$SO_2 + OH \xrightarrow{H_2O,O_2} H_2SO_4 + HO_2$$

Oxidation of SO_2 in the aerosol phase by catalytic reactions with O_2 and H_2O_2 is not considered here, but could easily be included in the model formulation.

MODEL APPLICATION

We will compute the formation of aerosol along an air trajectory in the Los Angeles basin on August 31, 1982 that started at about 1300 (PST) at Anaheim and arrived at Rubidoux between 1700 and 1800 (Fig. 1). For the simulation of the thermodynamic equilibrium between the particulate and gas phases the Kelvin effect has been neglected. The EQUIL model will be used for the base case calculation. A simulation will also be performed with the MARS model to compare the relative prediction accuracy and computational cost of these two thermodynamic submodels.

Gas and aerosol phase monitoring data are available at these locations against which to compare the predictions of our model. Emission rates, relative humidity, temperature, mixing depth and wind speed data are available for August 31, 1982 (Hildelmann et al

1984). Temperature was in the range 25 to 31° C, while relative humidity varied from 30% to 40%. Fig. 2 shows the initial size composition distribution determined on the basis of chemical equilibrium at Anaheim at 1300.

The measured and predicted concentrations at Rubidoux are given in Table 2. The predicted NO_2 concentrations have been corrected to include the other nitrogen containing species that interfere with the NO_2 measurement (Winer et al 1974). The resulting NO_2 prediction is slightly lower than the measured concentrations at Rubidoux. The predicted concentration for O_3 matches the observed value, while NH_3 matches the measured values at Rubidoux within the measurement uncertainties. Comparison of the predicted and observed sulfate, nitrate, and ammonium concentrations at Rubidoux indicates that we have adequately represented the formation of those aerosol species along the trajectory.

The evolution of the total sulfate-nitrate-ammonium concentrations along the trajectory is presented in Fig 3. The first few hours, due to the substantial quantity of hydroxyl radical in the atmosphere, SO_2 is predicted to react relatively rapidly to produce sulfuric acid in the gas phase, which then transfers to the aerosol phase. Thus, the sulfate aerosol mass keeps increasing until it reaches a maximum of about 7 $\mu g\, m^{-3}$ at about 1600, between Anaheim and Rubidoux. Late in the afternoon, the reduction in the photochemical activity causes a decrease in the hydroxyl radical concentration, resulting in a reduction of the production rate of sulfuric acid in the gas-phase. Hence turbulent diffusion and deposition predominate and the sulfate aerosol concentration declines smoothly to about 6.5 $\mu g\, m^{-3}$ at Rubidoux.

As shown in Table 5, condensation of sulfuric acid is the predominant source of sulfate mass increase in the aerosol phase, while dry deposition and eddy diffusion to the upper layers are the major removal mechanisms for aerosol sulfates. Since the ambient relative humidity on August 31, 1982 was very low, about 40%, the rate of particle formation, due

to binary nucleation is negligible and no new particles are predicted to be produced.

The predicted aerosol nitrate has its minimum at about 1330, near Anaheim. At that time the ambient temperature reaches its maximum of about 31° C. Such high temperature does not favor the formation of aerosol ammonium nitrate, and most of the nitrate exists in the gas-phase as nitric acid.

Later in the afternoon, near Rubidoux, the substantial increase in the ammonia concentration, due to production near Riverside, combined with a decrease of the ambient temperature to about 25° C, cause ammonia and nitric acid to condense as ammonium nitrate. Thus, both the ammonium and nitrate concentrations increase sharply and reach their maxima at about 1800, near Rubidoux.

Effect of Thermodynamic Submodel

In Table 1 we indicated that two size-independent thermodynamic submodels are available, EQUIL and MARS. Figure 3 shows the aerosol sulfate, nitrate, and ammonium concentrations calculated by using both these submodels. Since the sulfate concentration is controlled by gas-phase reaction and gas-to-particle diffusion, the sulfate prediction is unaffected by the choice of thermodynamic model.

The nitrate predictions differ between the two thermodynamic submodels. The curve corresponding to MARS shows lower nitrate concentrations along the course of the trajectory until close to Rubidoux. The reason for this difference is that EQUIL takes into account the existence of two mixed salts, $(NH_4)_2SO_4 \bullet 2NH_4NO_3$ and $(NH_4)_2SO_4 \bullet 3NH_4NO_3$, whereas MARS does not. As a result, at low relative humidities, whenever ammonia is in high enough concentration to form $(NH_4)_2SO_4$, but not so abundant to form pure solid NH_4NO_3, MARS predicts that no nitrates should be present in the aerosol phase. On the other hand, under the same conditions EQUIL predicts that nitrates exist in the solid phase in the form of mixed salts.

Near Rubidoux, due to the large production of ammonia in the eastern portion of the Los Angeles basin, the ammonium nitrate solid phase becomes thermodynamically favored. As a result, MARS predicts fairly well the existence of nitrates in the aerosol phase. EQUIL also predicts accurately the nitrate concentration over Rubidoux, showing, as presented in Fig. 4, that most of the nitrate is in the form of $(NH_4)_2SO_4 \bullet 3NH_4NO_3$.

Computationally the program that uses MARS is considerably faster than the one using EQUIL. For the specific trajectory examined here, the first one consumed 3 hours of CPU time, while the second one 4.5 hours of CPU time, on a VAX 11/780 . Therefore MARS, even though less accurate than EQUIL, might be preferred in an Eulerian regional air quality model, where computational efficiency is of paramount importance.

ANALYSIS OF MODEL SENSITIVITY

We now focus on an analysis of parameters that affect the aerosol chemical composition and size distribution. This sensitivity analysis was conducted using the EQUIL submodel. The parameters studied are NH_3 initial conditions and emissions, ambient temperature and relative humidity, together with initial aerosol and SO_2 concentrations. Table 3 summarizes the sensitivity tests we will present with the changes of the various parameters from their base case values, while Table 4 presents the results of the sensitivity runs for major species and aerosol concentrations, at Rubidoux.

The first sensitivity test examines the effect of the ammonia concentration on the formation of aerosols. In this test both the initial ammonia concentration and the ammonia emissions along the course of the trajectory were reduced by 50%. The resulting size-composition distribution at Rubidoux is shown in Figure 5. As expected, the sulfate concentration remains unaffected. An interesting point is that the pure ammonium nitrate phase decreases more than 50%, causing an overall 30% reduction of the nitrate mass and a 23% reduction in the ammonium mass, while the ammonium nitrate, that is contained

in the mixed salt, remains, practically, unaffected.

The second sensitivity test was designed to examine the influence of temperature on the aerosol formation and chemical composition. The ambient temperature was increased by 3° C. The resulting size-composition distribution at Rubidoux is shown in Figure 6. The sulfate mass in the aerosol phase is not seriously affected (only 1.5% increase from the Base case). The pure ammonium nitrate phase decreases more than 50% as the result of the increase in temperature, due to the strong temperature dependence of the ammonium nitrate dissociation constant.

In these two sensitivity tests condensational growth is the only route of gas-to-particle conversion (Table 5). The last sensitivity test was designed to investigate conditions under which nucleation is a pathway for gas-to-particle conversion, thus we selected a high humidity situation with the initial concentration of preexisting aerosol very low. The initial sulfate concentration was reduced to 0.004 $\mu g\, m^{-3}$, while the SO_2 concentration was increased by a factor of ten and the relative humidity maintained at 95%.

The resulting size-composition distribution at Rubidoux is presented in Figure 7. It is clear that the physical state of the resulting aerosol is completely different from the previous cases. Since the relative humidity is higher than the deliquescence humidity of all the possible salts, the aerosol consists of an aqueous solution of sulfate, nitrate and ammonium ions. The increased SO_2 concentration causes a substantial increase in the sulfate mass, and, as presented in Table 4, the overall sulfate concentration has been tripled, as compared to the previous cases. The total aerosol mass has been increased by an order of magnitude, as compared to the base case, basically due to the 400 $\mu g\, m^{-3}$ of condensed water.

As it is shown in Table 5, in contrast to the previous cases, here, nucleation does take place. High relative humidity provides a more favorable condition for nucleation. The

critical cluster contains many more water molecules per molecule of sulfuric acid than it does in low relative humidities. Therefore, lower sulfuric acid partial pressure is necessary for binary nucleation to occur, at the same rate, in humid environments than in dry ones.

What is crucial, though, for the formation of new particles by nucleation is the concentration of preexisting aerosol particles. The cleaner environment provides less total surface area of aerosols, hence there is less consumption of sulfuric acid vapors by condensation and, therefore, more H_2SO_4 available for nucleation (Middleton and Kiang 1978). In this sensitivity test all the new particle production by nucleation took place in the first thirty minutes of the simulation, when the concentration of preexisting aerosol was relatively low. After that time, the increasing aerosol mass accelerated the condensation process, resulting in no further particle production by nucleation. Under urban conditions, though, since background aerosol is always present, homogeneous nucleation of H_2SO_4-H_2O appears to be negligible.

New particles formed by nucleation are very small and do not contribute substantially to the total aerosol mass. They do, though, affect the number concentation density function in the range below 0.01 μm. In this sensitivity test, for example, the 0.023 $\mu g\, m^{-3}$ of sulfate produced by nucleation corresponds to about 10^{11} particles per cubic meter, one order of magnitude more than that initially existing in the system. Since the coagulation process is strongly dependent on the particle number density, these small particles move rapidly into the higher sections by coagulating among themselves and with preexisting small particles. This is the reason no particles smaller than 0.05 μm are predicted to exist when the trajectory reaches Rubidoux, as presented in Fig. 7.

CONCLUSIONS

A mathematical model that describes the evolution of the size and chemical composition distribution of atmospheric aerosols has been developed. The model, based on a

sectional representation of the size distribution, treats dynamics and thermodynamics of multicomponent atmospheric aerosols, including new particle formation by homogeneous heteromolecular nucleation, gas-to-particle conversion, coagulation and dry deposition.

The aerosol model was used to simulate the aerosol size and chemical composition on a trajectory from Anaheim to Rubidoux in the Los Angeles basin, for which measured particulate concentrations were available. Comparison between the predicted and observed aerosol concentrations showed that the model adequately predicted the concentrations of the major particulate compounds along that trajectory.

The particular day of the trajectory in question was characterized by low relative humidity, and as a result the aerosol consisted solely of dry ammonium sulfate and ammonium nitrate. The results of the simulation showed that mixed salts rather than pure phases were thermodynamically favored along the course of the trajectory.

Three tests were conducted to investigate the sensitivity of the model to various atmospheric parameters. As expected, reduction of the ammonia and increase in the ambient temperature cause a decrease in the aerosol ammonium nitrate concentration. Although a condition of high relative humidity, combined with very low initial aerosol concentration, leads to the formation of new particles, by nucleation, condensation is predicted to be the predominant mechanism for gas-to-particle conversion.

Future studies to be carried out with the model include extension to organic aerosols and evaluation of the effect of proposed control strategies on atmospheric aerosol levels.

ACKNOWLEDGMENT

This work was supported by State of California Air Resources Board Agreement A4-146-32 to the California Institute of Technology and by U.S Environmental Protection Agency contract 68-02-4076 to Systems Applications, Inc. Although the research described in this article has been funded in part by the U.S Environmental Protection Agency, it

does not necessarily reflect the views of the agency and no official endorsement should be inferred.

REFERENCES

Bassett M.E., Gelbard F. and Seinfeld J.H. (1981) Mathematical model for multicomponent aerosol formation and growth in plumes. Atmospheric Environment 15, 2395-2406.

Bassett M.E. and Seinfeld J.H. (1983) Atmospheric equilibrium model of sulfate and nitrate aerosol. Atmospheric Environment 17, 2237-2252.

Bassett M.E. and Seinfeld J.H. (1984) Atmospheric equilibrium model of sulfate and nitrate aerosol-II. Particle size analysis. Atmospheric Environment 18, 1163-1170.

Eltgroth M. W. and Hobbs P. V. (1979) Evolution of particles in the plumes of coal-fired power plants- II. A numerical model and comparison with field measurements. Atmospheric Environment 13, 953-975

Fuchs N.A. and Sutugin A.G. (1971) in Topics in Current Aerosol Research, G.M. Hidy and J.R. Brock, eds. Pergamon Press, Oxford, Vol. II, 1-60.

Gelbard F. and Seinfeld J.H. (1978) Numerical solution of the dynamic equation for particulate systems. J. Computational Physics 28, 357-375.

Gelbard F. and Seinfeld J.H. (1979) The general dynamic equation for aerosols-theory and application to aerosol formation and growth. J. Colloid Interface Sci. 69, 363-382.

Gelbard F. and Seinfeld J.H. (1980) Simulation of multicomponent aerosol dynamics. J. Colloid Interface Sci. 78, 485-501.

Gelbard F., Tambour Y. and Seinfeld J.H. (1980) Sectional representation for simulating aerosol dynamics. J. Colloid Interface Sci. 76, 541-556

Gelbard F. MAEROS (1984) Aerosol Science and Technology 3, 117-118.

Gmitro J. I. and Vermeulen T. (1964) Vapor-liquid equilibrium for aqueous sulfuric acid. AIChE J. 10, 740-746.

Harrison R. M. and Sturges W. T. (1984). Physico-chemical speciation and transformation reactions of particulate atmospheric nitrogen and sulfur compounds. Atmospheric Environment 18, 1829-1833.

Hildelmann L. M., Russell A.G. and Cass G.R. (1984) Ammonia and nitric acid concentrations in equilibrium with atmospheric aerosols: Experiment vs. theory. Atmospheric Environment 18, 1737-1750.

Liu M. K. and Seinfeld J. H. (1975) On the validity of grid and trajectory models of urban air pollution. Atmospheric Environment 9, 555-574.

Middleton P. and Brock J. (1976) Simulation of aerosol kinetics. J. Colloid Interface Sci. 54, 249-264.

Middleton P. and Kiang C.S. (1978) A kinetic aerosol model for the formation and growth of secondary sulfuric acid particles. J. Aerosol Sci. 9, 359-385.

Middleton P., Kiang C. S. and Mohnen V. A. (1980) Theoretical estimates of the relative importance of various urban sulfate aerosol production mechanisms. Atmospheric Environment 14, 463-472.

Mirabel P. and Katz J. L. (1974) Binary homogeneous nucleation as a mechanism for the formation of aerosols. J. Chem. Phys., 60, 1138-1144.

Perry R. H. and Chilton C. H. (1973) Chemical Engineers' Handbook, McGraw-Hill, New York, 5^{th} edition, 3-80, 3-81.

Russell A.G., McRae G. J. and Cass G. R. (1983) Mathematical modeling of the formation and transport of ammonium nitrate aerosol. Atmospheric Environment 17, 949-964.

Russell A.G. and Cass G. R. (1984) Aquisition of regional air quality model validation data for nitrate, sulfate, ammonium ions, and their precursors. Atmospheric Environment 18, 1815-1827.

Sabinina L. and Terpugow L. (1935) Die oberflächenspannung des systems schwefelsäure-wasser. Z. Phys. Chem. A173, 237.

Saxena P., Hudischewskyj A. B., Seigneur C. and Seinfeld J. H. (1986) A comparative study of equilibrium approaches to the chemical characterization of secondary aerosols. Atmospheric Environment 20, XXX-XXX.

Seigneur C. (1982) A model of sulfate aerosol dynamics in atmospheric plumes. Atmospheric Environment 16, 2207-2228.

Seigneur C., Hudischewskyj A. B., Seinfeld J. H. Whitby K. T., Whitby E.R., Brock J. R., and Barnes H. M. (1986) Simulation of aerosol dynamics: comparative review of mathematical models. Aerosol Science and Technology 5, XXX-XXX.

Seinfeld J. H. (1986) Atmospheric Chemistry and Physics of Air Pollution, John Wiley, New York.

Stelson A. W., Friedlander S. K. and Seinfeld J. H. (1979) A note on the equilibrium relationship between ammonia and nitric acid and particulate ammonium nitrate. Atmospheric Environment 13, 369-371.

Stelson A. W. and Seinfeld J. H. (1982a) Relative humidity and temperature dependence of the ammonium nitrate dissociation constant. Atmospheric Environment 16, 983-992.

Stelson A. W. and Seinfeld J. H. (1982b) Relative humidity and pH dependence of the vapor pressure of ammonium nitrate-nitric acid solutions at 25° C. Atmospheric Environment 16, 993-1000.

Stelson A. W. and Seinfeld J. H. (1982c) Thermodynamic prediction of the wa-

ter activity, NH_4NO_3 dissociation constant, density and refractive index for the NH_4NO_3-$(NH_4)_2SO_4$-H_2O system at 25° C. Atmospheric Environment 16, 2507-2514.

Suck S.H. and Brock J.R. (1979) Evolution of atmospheric aerosol particle size distributions via Brownian coagulation: Numerical simulation. J. Aerosol Sci. 10, 581-590.

Tanner R. L. (1982) An ambient experimental study of phase equilibrium in the atmospheric system: Aerosol-H^+, NH_4^+, SO_4^{2-}, NO_3^--$NH_{3(g)}$, $HNO_{3(g)}$. Atmospheric Environment 16, 2935-2942

Tilden J. W. and Seinfeld J. H. (1982) Sensitivity analysis of a mathematical model of photochemical air pollution. Atmospheric Environment 16, 1357-1364.

Tsang T. H. and Brock J. R. (1982) Aerosol coagulation from a crosswind line source. Atmospheric Environment 16, 2229-2235.

Tsang T. H. and Brock J. R. (1983) Simulation of aerosol growth by condensation and evaporation. Aerosol Sci. and Technology 2, 311-320.

Warren D. R. and Seinfeld J. H. (1985) Simulation of aerosol size distribution evolution in systems with simultaneous nucleation, condensation and coagulation. Aerosol Sci. and Technology 4, 31-43.

Winer A. M., Peters J. W., Smith J. P. and Pitts J. N. (1974) Response of commercial chemiluminescent NO-NO_2 analyzers to other nitrogen containing compounds. Environ. Sci. Technol., 8, 1118-1121.

Yue G. K. and Hamill P. (1979) The homogeneous nucleation of H_2SO_4-H_2O aerosol particles in air. J. Aerosol Sci. 10, 609-614.

Table 1. Computer Codes for Aerosol Sulfate/ Nitrate/ Ammonium/ Water Equilibria.

	KEQUIL[a]	EQUIL[b]	MARS[c]
Method used	Minimization of the Gibbs free energy,using conjugate gradient and Newton's methods. Use of homotopy method, to include the Kelvin effect.	Minimization of the Gibbs free energy,using conjugate gradient and Newton's methods.	The domain of feasible solutions is divided into several subdomains. Then the Gibbs free energy is minimized into the specific subdomain that corresponds to the given atmospheric conditions.
Kelvin effect	Included	Not included	Not included
Mixed salts	Included	Included	Not included
Aqueous phase reactions	Not included	Not included	Included
Typical simulation time for an equilibrium calculation[d]. (CPU sec.)	72	10	0.2

(Table 1 continued)

a) Bassett and Seinfeld (1984)

b) Bassett and Seinfeld (1983)

c) Saxena et al (1986)

d) Saxena et al (1986)

Table 2. Measured and Predicted Gaseous and Particulate Concentrations at Rubidoux, CA at 1700-1800 hours on August 31, 1982.

Species	Concentration	
	Measured	Predicted
NO_3^- ($\mu g\, m^{-3}$)	14.2-29.8	24.9
NH_4^+ ($\mu g\, m^{-3}$)	11.2-14.7	9.6
SO_4^{2-} ($\mu g\, m^{-3}$)	4.3-16.9	6.5
O_3 (ppb)	130.0	125.0
NO_2 (ppb)	50.0	31.0
SO_2 (ppb)	10	7.1
HNO_3 (ppb)	1.8-5.3	1.0
NH_3 (ppb)	59.8-89.0	58.0

Table 3. Parameters Varied in Sensitivity Study.

Sensitivity Study	Parameter	Variation
1	NH_3 initial conc. and emissions	50% decrease
2	Temperature	3° C increase
3	Relative humidity	increase to 95%
	SO_2 initial concentration	factor of 10 increase
	Initial sulfate concentration	factor of 10^3 decrease

Table 4. Predicted Gaseous and Particulate Concentrations at Rubidoux, CA for the Sensitivity Studies.

	Base case	Test 1	Test 2	Test 3
SO_4^{2-} ($\mu g\, m^{-3}$)	6.5	6.5	6.6	20.7
NO_3^- ($\mu g\, m^{-3}$)	24.9	17.6	20.0	30.8
NH_4^+ ($\mu g\, m^{-3}$)	9.6	7.4	8.2	16.5
H_2O ($\mu g\, m^{-3}$)	0.0	0.0	0.0	400.0
Total mass ($\mu g\, m^{-3}$)	41.0	31.5	34.8	468.0
SO_2 (ppb)	7.1	7.0	7.0	42.0
HNO_3 (ppb)	1.0	2.1	1.8	0.04
NH_3 (ppb)	58.0	25.0	60.0	43.8

Table 5. Contribution of Nucleation, Condensation, and Loss by Deposition.

($\mu g\, m^{-3}$)

		Sensitivity study		
	Base case	1	2	3
Initial	4.0	4.0	4.0	0.004
Nucleation	0.0	0.0	0.0	0.023
Condensation	4.85	4.85	4.96	29.06
Loss by deposition	-2.35	-2.35	-2.36	-8.38
Final	6.50	6.50	6.60	20.71

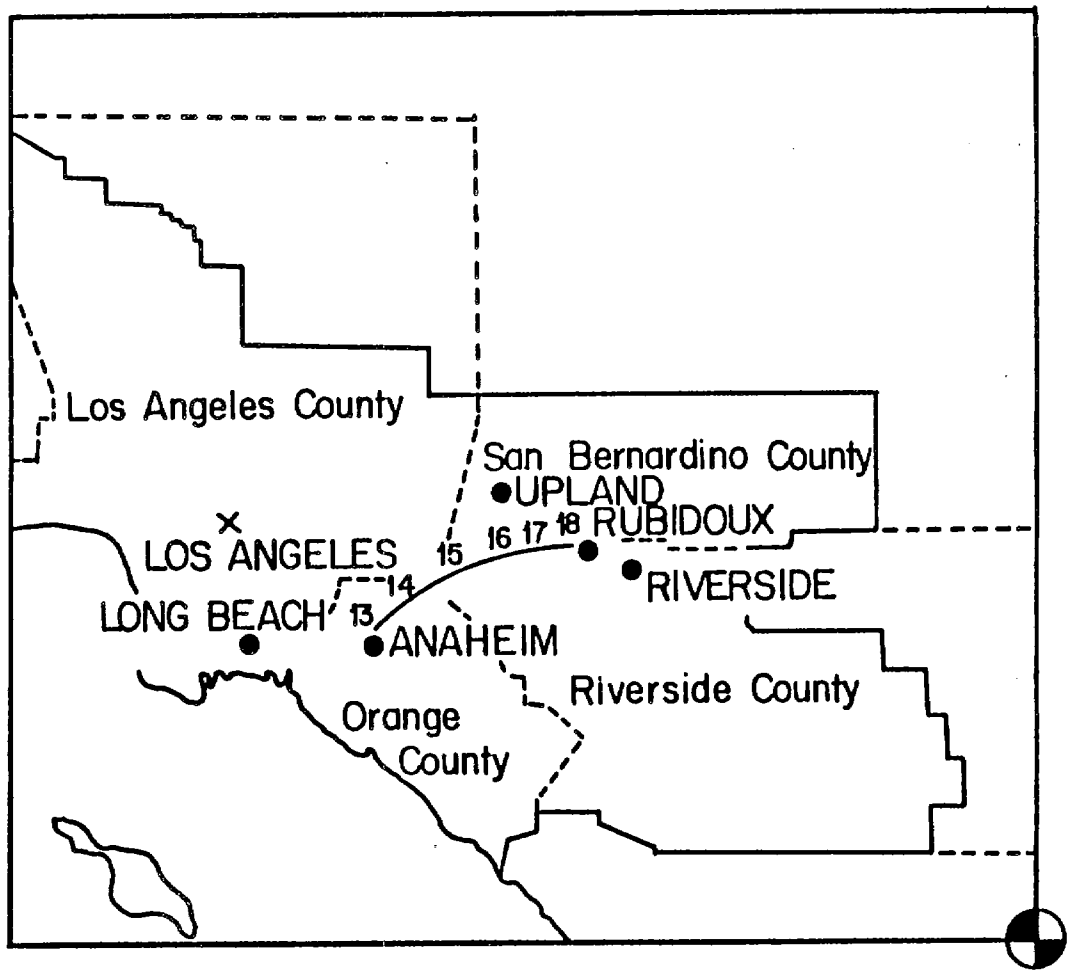

Fig. 1 Trajectory of the air mass that started on August 31,1982 at 1300 (PST) at Anaheim, CA and arrived at Rubidoux, CA at about 1800.

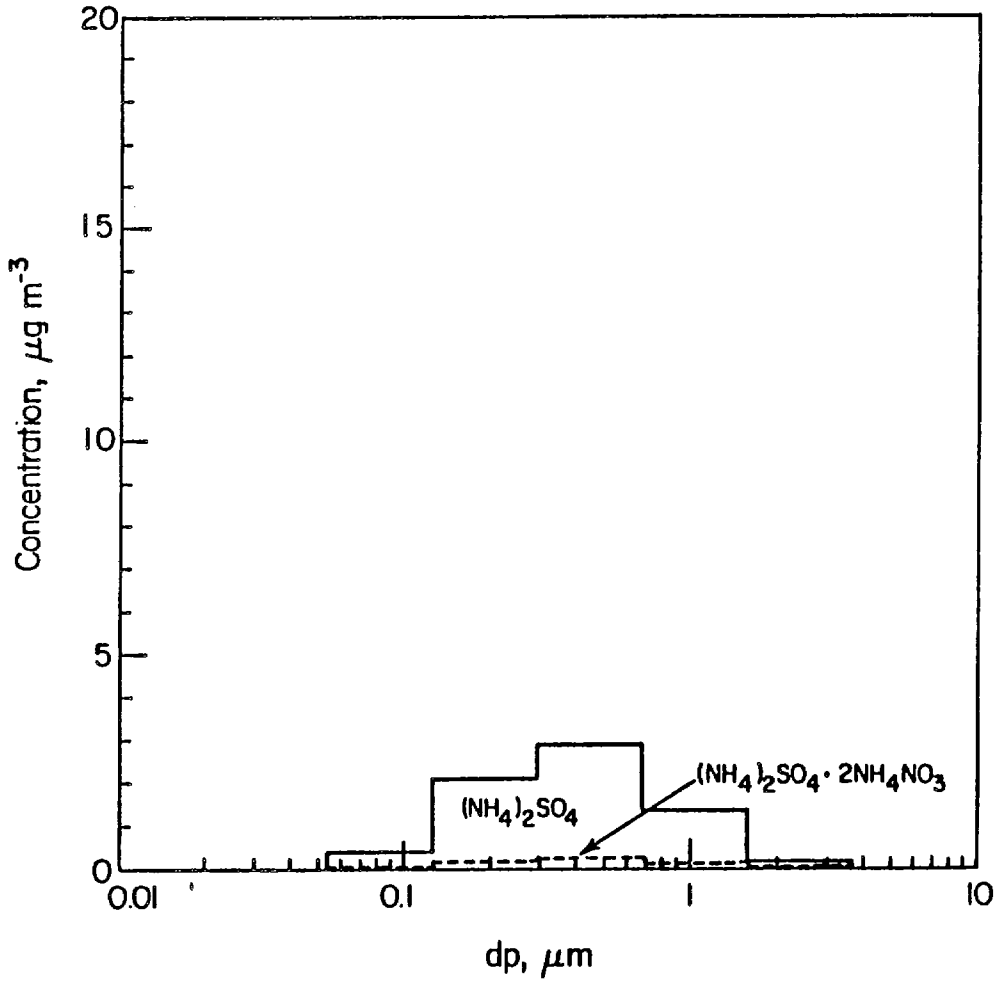

Fig. 2 Calculated aerosol size-composition distribution at Anaheim, CA at 1300 hours on August 31, 1982. The aerosol mass is an external mixture of $(NH_4)_2SO_4 \cdot 2NH_4NO_3$ and $(NH_4)_2SO_4$. The mass below the solid line indicates the total amount of aerosol, and the incremental components of that total are indicated.

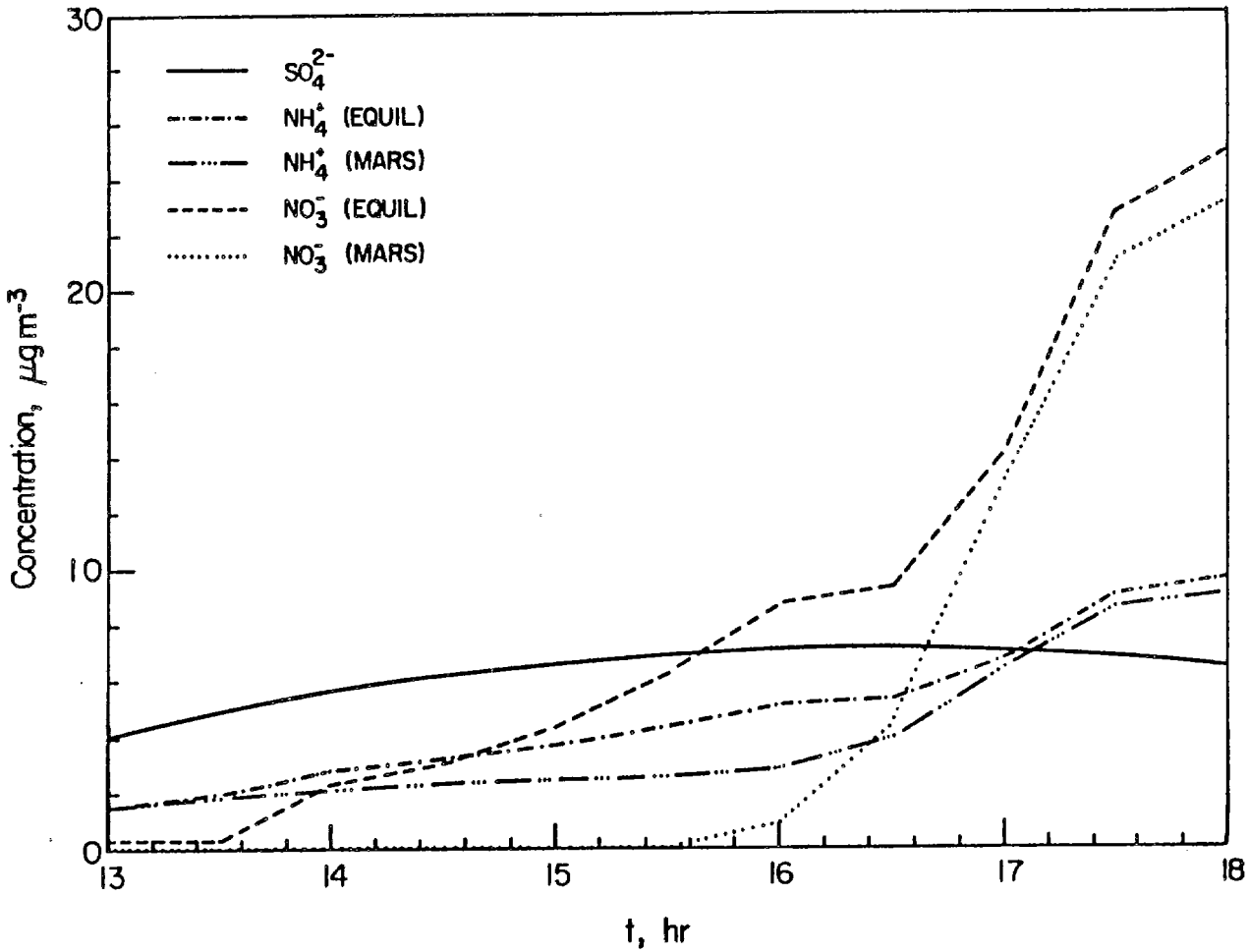

Fig. 3 Predicted evolution of total aerosol nitrate, ammonium and sulfate along the trajectory from Anaheim to Rubidoux, CA from 1300 to 1800 hours on August 31, 1982. Predictions are shown for the two thermodynamic models, EQUIL and MARS (Table 1).

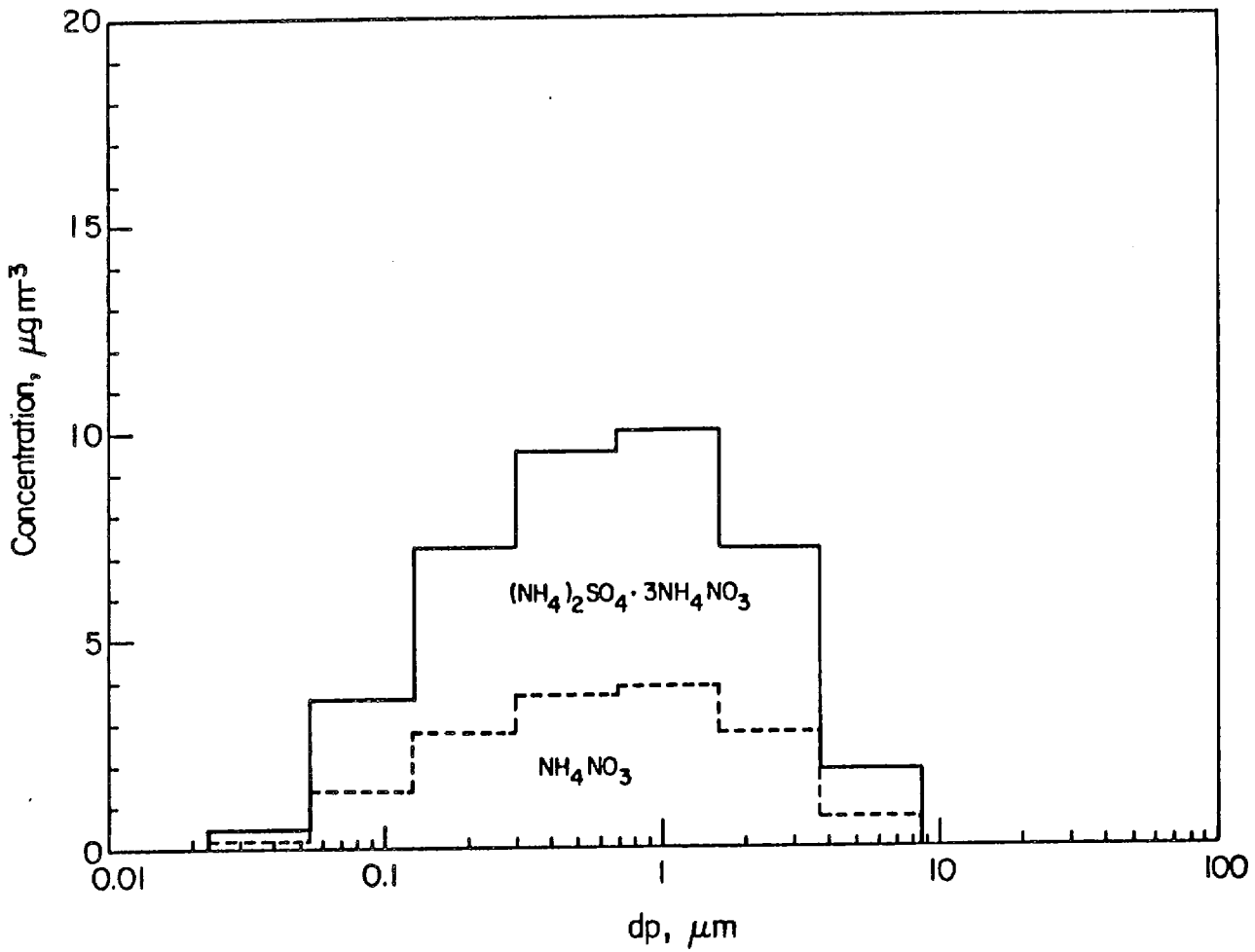

Fig. 4 Predicted size-composition distribution at Rubidoux, CA at 1800 hours on August 31, 1982. The aerosol mass is an external mixture of $(NH_4)_2SO_4 \bullet 3NH_4NO_3$ and NH_4NO_3. The mass below the solid line indicates the total amount of aerosol, and the incremental components of that total are indicated.

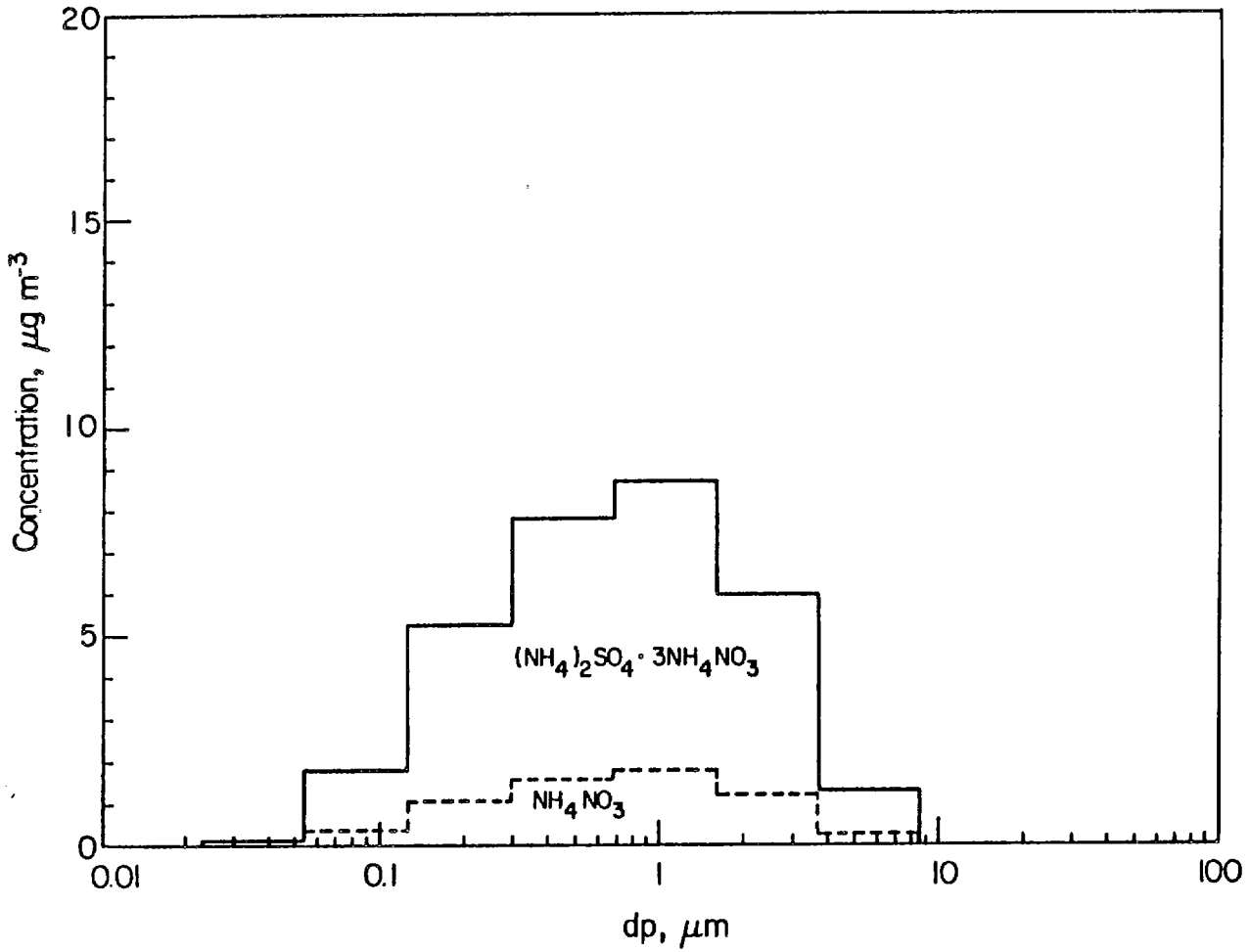

Fig. 5 Predicted size-composition distribution at Rubidoux, CA at 1800 hours on August 31, 1982. Conditions changed according to Test 1 in Table 3, namely 50% decrease in initial concentration and emission level of NH_3 from those of the base case, Figure 4. The aerosol mass is an external mixture of $(NH_4)_2SO_4 \bullet 3NH_4NO_3$ and NH_4NO_3. The mass below the solid line indicates the total amount of aerosol, and the incremental components of that total are indicated.

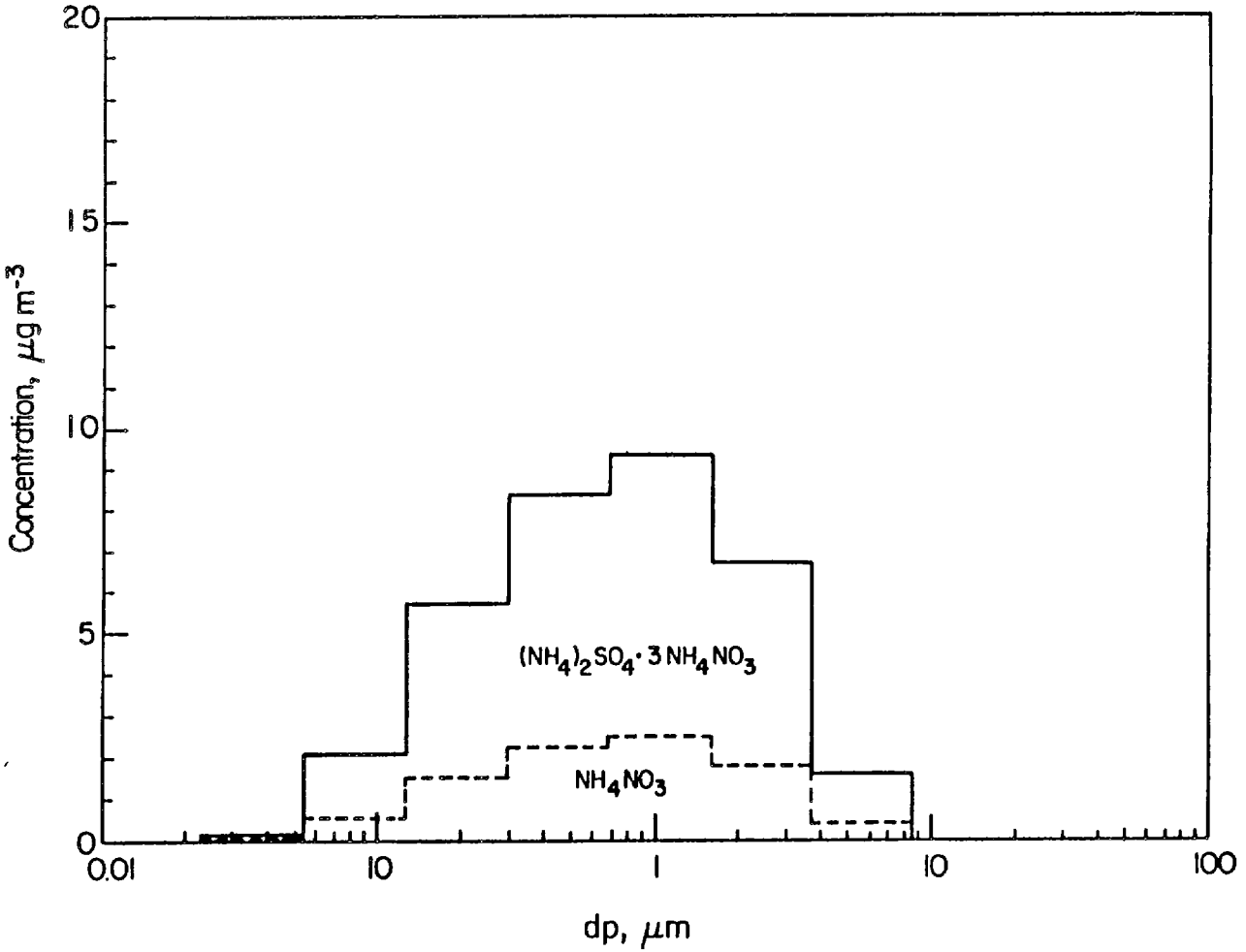

Fig. 6 Predicted size-composition distribution at Rubidoux, CA at 1800 hours on August 31, 1982. Conditions changed according to Test 2 in Table 3, namely 3° C increase in temperature from that of the base case, Figure 4. The aerosol mass is an external mixture of $(NH_4)_2SO_4 \bullet 3NH_4NO_3$ and NH_4NO_3. The mass below the solid line indicates the total amount of aerosol, and the incremental components of that total are indicated.

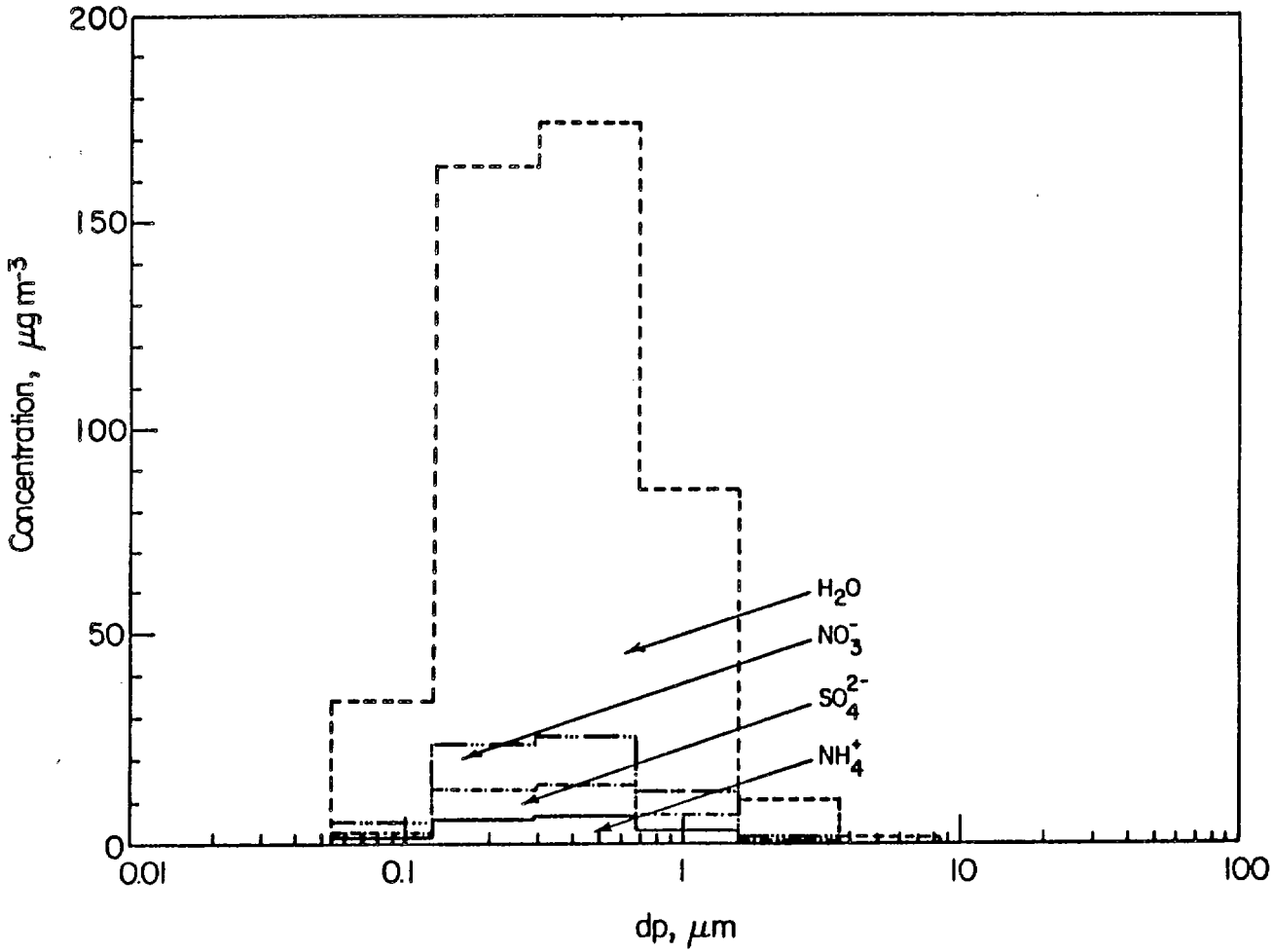

Fig. 7 Predicted size-composition distribution at Rubidoux, CA at 1800 hours on August 31, 1982. Conditions changed according to Test 3 in Table 3, namely increase of the relative humidity to 95%, increase of the initial SO_2 concentration by a factor of 10, and decrease of the initial sulfate level by a factor of 1000 from those of the base case, Figure 4. The aerosol consists of an aqueous solution of sulfate, nitrate, and ammonium ions. The mass below the upper line indicates the total amount of aerosol, and the incremental components of that total are indicated.

CHAPTER 3

CONTINUED DEVELOPMENT OF A GENERAL EQUILIBRIUM MODEL FOR INORGANIC MULTICOMPONENT ATMOSPHERIC AEROSOLS

CONTINUED DEVELOPMENT OF A GENERAL EQUILIBRIUM MODEL FOR INORGANIC MULTICOMPONENT ATMOSPHERIC AEROSOLS

CHRISTODOULOS PILINIS

Environmental Quality Laboratory

California Institute of Technology

Pasadena, CA 91125

and

JOHN H. SEINFELD

Department of Chemical Engineering

California Institute of Technology

Pasadena, CA 91125

ABSTRACT

A model is presented that predicts the total quantities of ammonium, chloride, nitrate and water contained in atmospheric aerosols, their physical state and their distribution among aerosol particles of different sizes. The model is based on the thermodynamic equilibrium calculation of the ammonium chloride, nitrate, sodium, sulfate, water system. The existence of water in the aerosol phase at low relative humidities is shown to be explained. Observed aerosol concentrations at Long Beach, California during August 30-31, 1982 are successfully predicted.

KEY WORD INDEX

Aerosol, inorganic. Water, in atmospheric aerosols. Sodium chloride.

INTRODUCTION

Atmospheric aerosols consist of solid and/ or liquid multicomponent particles. Prevalent compounds of both urban and natural aerosols are sulfate, nitrate, ammonium, sodium, chloride, water, organics and trace metals (Hitchcock et al, 1980; Russell and Cass, 1984; Jacob et al 1985; John et al 1987). A major question underlying understanding the chemical nature of the atmospheric aerosol is- what is the relationship among the chemical constituents of the aerosol. Early work by Stelson et al (Stelson et al, 1979; Stelson and Seinfeld, 1982abc) and further work by others (Bassett and Seinfeld, 1983 and 1984; Saxena et al, 1983; Seigneur and Saxena 1984; Saxena et al 1986) have postulated that the sulfate/ nitrate/ ammonium aerosol constituents should be in thermodynamic equilibrium with the local gas phase. Ambient measurements reported by a number of investigators (Hildelmann et al 1984, John et al 1985) have generally confirmed the equilibrium relationship among these species, although it has been shown that the thermodynamic equilibrium models for the sulfate/ nitrate/ ammonium system consistently underpredict the nitrate concentrations in the aerosol phase (Hildelmann et al, 1984; Jacob et al, 1986).

Drawing on previous work on the thermodynamics of the sulfate/ nitrate/ ammonium system (Bassett and Seinfeld, 1983, 1984; Saxena et al 1986) Pilinis et al (1987) presented an urban multicomponent aerosol model. Formulated in a trajectory framework, the model assumed that aerosol sulfate and organic levels are controlled by gas-to-particle conversion (condensation and nucleation), while particulate ammonium and nitrate concentrations are governed by thermodynamic

equilibrium.

For a number of reasons, however, these thermodynamic models are incomplete in representing the general atmospheric aerosol. A notable omission is sodium chloride (NaCl). Ambient measurements have shown that NaCl is present at substantial concentrations in regions close to oceans (Russell and Cass, 1984; Orsini et al, 1986; John et al, 1987; Wall et al, 1987). Moreover it has been observed that marine aerosol can exhibit up to 100% loss of its chloride due to its reaction with strong acids (H_2SO_4 and HNO_3) (Hitchcock et al, 1980), providing evidence of chemical interaction between NaCl and other atmospheric constituents.

A shortcoming of the previous thermodynamic treatments is that they fail to predict the larger median diameter for nitrates than for sulfates (Hidy et al, 1975). Bassett and Seinfeld (1984) speculated that the Kelvin effect might be responsible for this phenomenon. Their calculations, though, showed that, if the Kelvin effect was the cause, then inordinately long times would be needed for the thermodynamic equilibrium to be established. Furthermore, there is a strong correlation between the coarse NaCl primary aerosol and the existence of nitrates in the large particles (Wall et all, 1987).

An additional shortcoming of the previous thermodynamic models is that they cannot treat cases where various non-volatile species are non-uniformly distributed among particles of different sizes. Since in their thermodynamic treatment H_2SO_4 was the only non-volatile species, after the total amount of volatiles in the aerosol phase had been determined with thermodynamic arguments, they distributed the aerosol volatile species so that the ratio of volatiles to non-volatiles is constant for all the aerosol size sections. This approach, though, is not applicable in the case

where more than one non-volatile compounds lie in the aerosol phase.

The goal of the present paper is to present a more comprehensive thermodynamic model of atmospheric aerosols. The system is ammonium/ chloride/ nitrate/ sodium/ sulfate/ water including solid, liquid and gaseous phases. Since most of the particulate mass is associated with particles larger than 0.01μm, the Kelvin effect will be neglected. The sectional representation of the aerosol size composition distribution will be used and differences in the primary composition among different sections will be taken into account. The aerosol population in each section will be assumed to be an internal mixture of all the species involved, which means that all the particles in each section have exactly the same composition. At relative humidities below the deliquesence point of each of the various salts we include the equilibria between solid-ions using recent experimental values of binary activity coefficients and water activities of highly supersaturated solutions (Cohen et al, 1987ab). At relative humidities below the lowest deliquesence point of the thermodynamicaly possible salts the aerosol is assumed to be completely solid.

In the next two sections the basic theory on which the thermodynamic model is based and its application on the specific system will be presented. The subsequent section describes in detail a general method with which the differences in the composition among particles of different sizes may be taken into account. The rest of the paper consists of application of the model. First comparison is made with the previous models in terms of predicted concentrations, for just the ammonium/sulfate/nitrate system, for which the other models can be also applied. Then the model is used to predict the behavior of atmospheric aerosols and the

significance of the inclusion of NaCl, while in the last section the predictions of the model are compared to ambient aerosol concentrations observed in Los Angeles, California. An attempt will be also made to explain the observed lack of deliquesent behavior of atmospheric aerosols, as well as the existence of water in the aerosol phase at low relative humidities (Hänel et al, 1970; Covert et al, 1972; Winkler et al, 1973 and Ho et al 1974).

FORMULATION OF THE EQUILIBRIUM MODEL

The condition of chemical equilibrium in a closed system, such as the one under consideration, at constant temperature T and pressure p is that the total Gibbs free energy of the system G is a minimum. Therefore the problem addressed here, from a mathematical point of view, is a constrained minimization problem of the form:

$$\min_{n_i} G(T, p, n_i) \qquad \text{with} \quad n_i \geq 0 \tag{1}$$

where n_i, i =1,2,3... is the concentration of the i^{th} species in the system (in moles m^{-3} of air). Eq. (1) is satisfied for constant temperature and pressure if and only if (Denbigh, 1981)

$$\sum_i \nu_{ij}\mu_i = 0 \quad \text{for} \quad \text{all} \quad \text{reactions} \quad j \tag{2}$$

where, ν_{ij} is the stoichiometric coefficient of the i^{th} species in the j^{th} reaction and $\mu_i = (\frac{\partial G}{\partial n_i})_{\text{T,P},n_r}$ is the chemical potential of species i. To solve the system (2) expressions for the chemical potentials are needed, which are discussed in the next section.

1. Chemical Potentials and Equilibrium Constants

In general the chemical potential of species i is given by

$$\mu_i = \mu_i^0(T) + RT\ln a_i \tag{3}$$

where $\mu_i^0(T)$ is the standard chemical potential for 1 atm and temperature T (in K), R is the gas constant and a_i is the activity of the i^{th} species. For pure solid phases $a_i = 1$, for ideal gases $a_i = p_i$ where p_i is the partial pressure of the i^{th} species (in atmospheres) and for aqueous solutions of electrolytes $a_i = \gamma_i^{(\nu_+ + \nu_-)} m_+^{\nu_+} m_-^{\nu_-}$, where γ_i is the activity coefficient of species i in water, ν_+ and ν_- are the moles of cations and anions, respectively, released by one mole of the electrolyte, and m_+, m_- are the molalities of the cation and anion respectively. For electrolytes the standard chemical potential is related to the standard chemical potentials $\mu_{i+}^0(T)$ and $\mu_{i-}^0(T)$ of the cations and anions, respectively, $\mu_i^0(T) = \nu_+\mu_{i+}^0(T) + \nu_-\mu_{i-}^0(T)$.

Substituting (3) into (2) for μ_i and rearranging terms we find

$$\prod_i a_i^{\nu_{ij}} = K_j(T) \tag{4}$$

where $K_j(T)$ is the equilibrium constant of the j^{th} reaction,

$$K_j(T) = exp[-\frac{\sum_i \nu_{ij}\mu_i^0(T)}{RT}] \tag{5}$$

The system of equations (4) will be solved to determine the aerosol composition at thermodynamic equilibrium. To determine the activities of the various electrolytes, expressions for the activity coefficients of all the salts involved are needed.

At constant pressure the equilibrium constant K is function only of the temperature and it is expressed by the Van't Hoff's equation

$$\frac{d\ln K(T)}{dT} = \frac{\Delta H^o(T)}{RT^2} \tag{6}$$

where $\Delta H^o(T)$ is the corresponding standard enthalpy change of the reaction at temperature T (Denbigh, 1981). A good approximation of $\Delta H^o(T)$ is

$$\Delta H^o(T) = \Delta H^o(T_o) + \Delta c_p^o(T - T_o) \tag{7}$$

where $\Delta H^o(T_o)$ is the corresponding standard enthalpy change at the base temperature ($T_o = 298.1$K) and Δc_p^o is the change of the heat capacity at T_o. Substituting (7) for $\Delta H^o(T)$ in (6) and integrating we obtain

$$K(T) = K_o \exp\left[- \frac{\Delta H^o(T_o)}{RT_o}\left(\frac{T_o}{T} - 1\right) - \frac{\Delta c_p^o}{R}\left(1 + \ln(\frac{T_o}{T}) - \frac{T_o}{T}\right)\right] \tag{8}$$

where K_o is the equilibrium constant at T_o that can be found by (5) using tables of thermodynamic data (Wagman et al, 1968).

Finally, by applying the condition of phase equilibrium for water in (1) the water activity in the aqueous phase is found equal to the relative humidity RH, that is

$$a_w = \mathrm{RH} \qquad (0 \leq \mathrm{RH} \leq 1) \tag{9}$$

In the situation of interest to us the value of RH will be known (available from ambient measurements) and thus from (9) the water activity of any aqueous phase is fixed. The water activity a_w is a complex function of the individual ion and natural species concentrations, but that combination must be such that (9) is obeyed.

There are a number of theories that allow one to predict the water activity of a multicomponent aqueous electrolyte solution using binary data of solutions of either the same ionic strength or the same water activity as the multicomponent solution. Some of the widely used theories, such as RWR, RB, MK and ZSR, have been compared and tested with experimental data for many multicomponent solutions up to very high ionic strengths (Sangster and Lenzi, 1974; Saxena and Peterson, 1981; Cohen et al 1987ab). In most of the cases the water activities predicted with these methods do not differ by more than 5%. Thus the computationally favorable ZSR method was selected to be used.

The ZSR method may be described as follows (Robinson and Stokes, 1965). Given a multicomponent solution of individual molalities m_i, let $m_{0i}(a_w)$ be the molality of the binary solution of the i^{th} electrolyte in water of the same water activity as the multicomponent solution. Then the following equation is satisfied at equilibrium

$$\sum_i \frac{m_i}{m_{0i}(a_w)} = 1 \tag{10}$$

Equations (9) and (10) combined can be used to calculate the water content of atmospheric aerosols.

2. Activity Coefficients

Most of the methods that predict the activity coefficients of an electrolyte in a multicomponent solution use, in one way or another, the activity coefficients of binary mixtures of the same ionic strength for their predictions.

We use Bromley's model (Bromley; 1973), which has been used up to very high ionic strengths (Saxena and Peterson; 1981, Sangster and Lenzi; 1974). According

to this model

$$\log\gamma_{12} = -A_\gamma \frac{Z_1 Z_2 I^{1/2}}{1 + I^{1/2}} + \frac{Z_1 Z_2}{Z_1 + Z_2}\left[\frac{F_1}{Z_1} + \frac{F_2}{Z_2}\right] \tag{11}$$

where γ_{12} is the activity coefficient of cation 1 and anion 2, Z_1 and Z_2 are the absolute values of the charges of the ions of the electrolyte 12, $I = \frac{1}{2}\sum_i m_i Z_i^2$ is the ionic strength, $A_\gamma = 0.511$ kg$^{1/2}$mole$^{-1/2}$, and where

$$F_1 = Y_{21}\log\gamma_{12}^{\circ} + Y_{41}\log\gamma_{14}^{\circ} + Y_{61}\log\gamma_{16}^{\circ} + ...+$$
$$+\frac{A_\gamma I^{1/2}}{1 + I^{1/2}}[Z_1 Z_2 Y_{21} + Z_1 Z_4 Y_{41} + Z_1 Z_6 Y_{61} + ...] \tag{12}$$

and

$$F_2 = X_{12}\log\gamma_{12}^{\circ} + X_{32}\log\gamma_{32}^{\circ} + X_{52}\log\gamma_{52}^{\circ} + ...+$$
$$+\frac{A_\gamma I^{1/2}}{1 + I^{1/2}}[Z_1 Z_2 X_{12} + Z_3 Z_2 X_{32} + Z_5 Z_2 X_{52} + ...] \tag{13}$$

with

$$Y_{21} = \left(\frac{Z_1 + Z_2}{2}\right)^2 \frac{m_2}{I} \tag{14}$$

and

$$X_{12} = \left(\frac{Z_1 + Z_2}{2}\right)^2 \frac{m_1}{I} \tag{15}$$

In (11) through (15) the cations have the subscripts 1,2,3 etc. and the anions have 2,4,6 etc. Thus, to find the activity coefficients in the multicomponent solution with Bromley's method one needs to know the binary activity coefficients of all the possible pairs of anions and cations in a solution of the same ionic strength.

A widely used method to calculate binary activity coefficients is Pitzer's method (Pitzer and Mayorga; 1973), according to which

$$\ln\gamma_{12}^{\circ} = Z_1 Z_2 f^\gamma + m_{12}\frac{2\nu_1\nu_2}{\nu_1 + \nu_2} B_{12}^\gamma + m_{12}^2 \frac{2(\nu_1\nu_2)^{3/2}}{\nu_1 + \nu_2} C_{12}^\gamma \tag{16}$$

where ν_1 and ν_2 are the numbers of cations and anions in the electrolyte formula respectively, m_{12} is the molality of that electrolyte for the given ionic strength, and where

$$f^{\gamma} = -0.392\left[\frac{I^{1/2}}{1+1.2I^{1/2}} + \frac{2}{1.2}\ln(1+1.2I^{1/2})\right] \tag{17}$$

$$B_{12}^{\gamma} = 2\beta_{12}^{(0)} + \frac{2\beta_{12}^{(1)}}{4I}\left[1 - e^{-2I^{1/2}}(1+2I^{1/2}-2I)\right] \tag{18}$$

The $\beta_{12}^{(0)}$, $\beta_{12}^{(1)}$ and C_{12}^{γ} are semiempirical parameters, the values of which have been extracted by curve fitting of experimental data for various binary electrolyte solutions. For many of the salts involved in atmospheric aerosols these parameters have been recently updated so that they can apply up to very high ionic strengths (Cohen et al, 1987ab).

APPLICATION TO THE NH_3, NaCl, HCl, H_2SO_4, HNO_3, H_2O SYSTEM

The system we are considering consists of the following potential components:

Gas phase: NH_3, HCl, HNO_3, H_2O

Liquid phase: H_2O, NH_4^+, SO_4^{2-}, NO_3^-, H^+,
Na^+, Cl^-, HSO_4^- and H_2SO_4

Solid phase : Na_2SO_4, $NaHSO_4$, NaCl, $NaNO_3$, NH_4Cl,
NH_4NO_3, $(NH_4)_2SO_4$, NH_4HSO_4 and $(NH_4)_3H(SO_4)_2$

Table 1 summarizes the equilibria and the equilibrium constants that are relevant for this system.

The approach followed for the above system is the following. Since sulfuric acid has a very low vapor pressure it can be assumed to reside completely in the

aerosol phase where it may react with NaCl and NH_3. Thus the molar ratio of ammonia plus sodium chloride to sulfuric acid is of fundamental importance. The system is sulfate deficient if the ratio $R_{H_2SO_4} = \frac{m_{NH_3}+m_{NaCl}}{m_{H_2SO_4}} \geq 2$. On the other hand, it is sulfate rich, if $R_{H_2SO_4} < 2$.

In the sulfate deficient case sulfuric acid can be assumed to be completely neutralized, since there is an abundance of ammonia and sodium chloride. The sulfate rich case can be divided into two subcases. When $1 \leq R_{H_2SO_4} < 2$, part of the H_2SO_4 is neutralized, while the rest of it reacts to produce HSO_4^-. The ratio of HSO_4^- to SO_4^{2-} is controlled by thermodynamic equilibrium. When $R_{H_2SO_4} < 1$, the solution is very acidic. Part of the H_2SO_4 dissociates to HSO_4^-, while the rest remains as $H_2SO_{4(l)}$, the distribution governed by thermodynamic equilibrium.

Another important variable is the relative humidity of deliquesence. Table 2 summarizes the deliquesence relative humidities for the nine possible solids. The RH above mixed, saturated solutions is less than or equal to the relative humidity of deliquesence of the individual salts involved. Thus, for relative humidities above the deliquesence of a specific solid the solid may not exist. On the other hand, for humidities below the deliquesence RH the solid phase may or may not exist, depending on the thermodynamic equilibrium. Thus, the equilibrium between solid and ions in aqueous solution for that specific salt must be considered in order to examine whether any solid exists. For RH's lower than the lowest deliquesence relative humidity of the salts involved, the aerosol is assumed to be dry and only the equilibrium between the gas and the solid phases is taken into account.

Thus, the entire range of relative humidities can be divided into several regimes. Tables 3 and 4 show the possible compounds as a function of the relative

humidity for the sulfate deficient and sulfate rich cases respectively.

Given the concentrations of NaCl, NH_3, HNO_3 and H_2SO_4, as well as the RH and temperature, the possible compounds at equilibrium are identified using Tables 3 and 4. Then a combination of Newton Raphson and bisection methods is used to solve the system of equations (4) together with the mass conservation and electroneutrality constraints and (9) and (10) to determine the equilibrium physical state and composition of the mixture.

Binary water activities and activity coefficient parameters for most of the electrolytes are taken from recent experimental work (Cohen et al; 1987ab), while those for the rest of the species from Bassett and Seinfeld (1983) and Pitzer and Mayorga (1973). Tables 5 and 6 present the water activities and binary activity coefficient parameters, respectively, that were used in our calculations.

THE SECTIONAL EQUILIBRIUM MODEL

In the case of atmospheric aerosols the non-volatile species H_2SO_4 and NaCl are not uniformly distributed among particles of different sizes (Wall et al; 1987). As a result, different species might be thermodynamically favored in fine particles over coarse ones. Consider, for example, the case of an aerosol consisting of two sections, fine and coarse, with 0.1μmole of H_2SO_4 in the fine section and 0.2μmole of NaCl in the coarse section. If no specific account is made, the thermodynamic model will predict that, at equilibrium, the aerosol will consist of pure Na_2SO_4. We overcome this problem as follows.

At equilibrium, all the particles, regardless of their size are exposed to the same partial pressure of the volatile species. Let $p_0^{HNO_3}$ and $p_e^{HNO_3}$ be the initial

and the equilibrium partial pressures of HNO_3, that is to say the pressure before any reaction takes place and after the thermodynamic equilibrium is established, respectively. Then the mass balance equation for nitrates can be written

$$\frac{p_0^{HNO_3}}{RT} = \frac{p_e^{HNO_3}}{RT} + \sum_{i=1}^{L} c_i^{HNO_3} \tag{19}$$

where $c_i^{HNO_3}$ is the nitrate concentration in the i^{th} section and L is the total number of sections.

Let $w_i^{HNO_3}$ be a new variable, defined by

$$w_i^{HNO_3} = \frac{p_e^{HNO_3}}{RT} + c_i^{HNO_3} \tag{20}$$

Substituting (20) for $c_i^{HNO_3}$ into (19) one gets

$$\frac{p_0^{HNO_3}}{RT} = \sum_{i=1}^{L} w_i^{HNO_3} - (L-1)\frac{p_e^{HNO_3}}{RT} \tag{21}$$

Similarly for NH_3

$$\frac{p_0^{NH_3}}{RT} = \sum_{i=1}^{L} w_i^{NH_3} - (L-1)\frac{p_e^{NH_3}}{RT} \tag{22}$$

and for HCl

$$c_0^{HCl} = \sum_{i=1}^{L} w_i^{HCl} - (L-1)\frac{p_e^{HCl}}{RT} \tag{23}$$

where c_0^{HCl} is the total chloride concentration, that is the sum of the sodium chloride and HCl in the system.

Physically $w_i^{HNO_3}$, $w_i^{NH_3}$ and w_i^{HCl} are the hypothetical initial concentrations of HNO_3, NH_3 and HCl, respectively, that, in an atmosphere containing only the

non-volatiles of the i^{th} section, give the same equilibrium composition of this aerosol section, as well as the same equilibrium partial pressures of the volatiles as when $p_0^{HNO_3}$, $p_0^{NH_3}$ and c_0^{HCl} are applied over the total aerosol population. This property of w_i's is the most useful one, because it enables us to use the method described in the previous section to find the equilibrium composition of all the size sections.

One solves (21), (22) and (23) together with

$$\begin{aligned} p_e^{HNO_3} &= p_{ie}^{HNO_3}(w_i^{HNO_3}, w_i^{NH_3}, w_i^{HCl}) \\ p_e^{NH_3} &= p_{ie}^{NH_3}(w_i^{HNO_3}, w_i^{NH_3}, w_i^{HCl}) \\ p_e^{HCl} &= p_{ie}^{HCl}(w_i^{HNO_3}, w_i^{NH_3}, w_i^{HCl}) \end{aligned} \tag{24}$$

$$\text{for} \qquad i = 1, 2, ..., L$$

to find w's and p_e's, using the ZSPOW non-linear equation solver of the International Mathematical and Statistical Libraries (IMSL). In (24) $p_{ie}^{HNO_3}$, $p_{ie}^{NH_3}$ and p_{ie}^{HCl} are the equilibrium HNO_3, NH_3 and HCl partial pressures for the isolated system containing the H_2SO_4 and NaCl of the i^{th} section and the w_i's, at the given temperature and RH. These pressures are determined, at each step of ZSPOW, by solving, for each of the L size sections, the system of equations (4) together with the electroneutrality and mass balance conditions for each individual section; thus finding the physical state and chemical composition at equilibrium for each of the sections, for the current values of the w' s.

COMPARISON WITH EXISTING AEROSOL MODELS

We have presented a model to predict the equilibrium composition of the ammonium/sodium/sulfate/nitrate/water system, given the initial concentrations of H_2SO_4, HNO_3, NH_3, NaCl and HCl, the ambient RH and the ambient temperature. In the case of one section and zero NaCl concentration, we should obtain results similar to the other two existing aerosol equilibrium models, MARS and EQUIL that treat the NH_3, H_2SO_4, HNO_3 and H_2O system (Bassett and Seinfeld, 1983; Saxena et al, 1986). Table 7 shows the results of the simulations by the current program, SEQUILIB, together with the results of both MARS and EQUIL for relative humidities ranging from 51-91%. The input data are typical ambient concentrations, i.e. 10 μg m^{-3} H_2SO_4, 10 μg m^{-3} NH_3 and 30 μg m^{-3} HNO_3, while the ambient temperature was assumed to be 25°C (298 K).

As shown in Table 7, SEQUILIB gives results similar to both EQUIL and MARS over the whole range of relative humidities for all the species. MARS disagrees with the predictions of the other two programs in the case of 66% RH, where it predicts dry aerosol without any nitrate in the solid phase. Since for both 61% and 71% RH's MARS predicts the existence of aerosol nitrates, numerical difficulties in MARS probably are the cause of the discrepancy at 66% RH. The small differences of the water content in the aerosol phase for RH's higher than 66% is due to differences in the methods used to calculate the activity coefficients. For all the runs of Table 7 SEQUILIB needed 21 CPUs, while MARS needed 3CPUs and EQUIL 113CPUs on a VAX-11/780.

THE ROLE OF NaCl IN ATMOSPHERIC AEROSOLS

The model we have developed can be used to examine how NaCl affects the

concentration and physical state of a typical urban aerosol at both high and low relative humidities. The input data were again 10 μg m^{-3} H_2SO_4, 0 μg m^{-3} HCl, 10 μg m^{-3} NH_3 and 30 μg m^{-3} HNO_3, while the ambient temperature was assumed to be 25°C (298 K). The NaCl concentration was varied from 0-30 μg m^{-3}. Relative humidities of 90% and 40% will be considered. Only one aerosol size section is assumed.

Figure 1 shows the predicted aerosol composition for 90% relative humidity. Even at 0 μg m^{-3} NaCl, the high concentrations of H_2SO_4 and HNO_3 force all the ammonia into the aerosol phase. Since the relative humidity is high (90%) the aerosol is predicted to be an aqueous solution of sulfate, nitrate, chloride, sodium and ammonium ions. As the NaCl concentration increases, the nitrate concentration increases almost linearly with the increase in NaCl. This increase in nitrate is directly correlated with the increase of the NaCl concentration, because all the NH_3 already lies in the aerosol phase. As the NaCl concentration increases, water condenses to satisfy the thermodynamic equilibrium. As is shown in Fig. 1, the liquid water content also increases with the NaCl. One should mention at this point that, even though the relative humidity in this example is below the deliquesence point for Na_2SO_4, no solid sodium sulfate is predicted to coexist with the aqueous phase.

Figure 2 shows the predicted aerosol composition under the same conditions but for 40% RH. Because the ambient humidity is very low, the aerosol is predicted to be completely dry. We note that the effect of increasing NaCl concentration on the aerosol composition is quite different from the previous case. As the NaCl increases it reacts with the H_2SO_4 existing in the aerosol phase, forming Na_2SO_4.

Thus less H_2SO_4 is available to react with NH_3, resulting in a decreasing concentration of $(NH_4)_2SO_4$, until it becomes zero at about 12 μg m^{-3} NaCl. At this point NaCl consumes the total available H_2SO_4. The available NH_3 reacts primarily with HNO_3, producing NH_4NO_3. This is the reason the NH_4NO_3 concentration is predicted to have its maximum at exactly the same point, where the available H_2SO_4 is consumed. Beyond this point the NaCl concentration increase causes different results. Since H_2SO_4 has been completely consumed, the Na_2SO_4 concentration remains constant. The excess NaCl reacts with HNO_3 to produce $NaNO_3$. As more and more HNO_3 reacts to form $NaNO_3$, less remains to form NH_4NO_3 resulting in a decrease of the NH_4NO_3 concentration. At very high NaCl concentrations the HCl produced by the reactions involving NaCl reaches high enough levels to react with NH_3 to produce NH_4Cl.

The next figure shows the predicted aerosol composition by equivalents (%) for 15 μg m^{-3} NaCl, 10 μg m^{-3} NH_3 and 30 μg m^{-3} HNO_3, 90% RH and ambient temperature 298 K. The initial H_2SO_4 was 10 μg m^{-3} and 50 μg m^{-3} for cases (a) and (b) respectively. Case (a) corresponds to a sulfate deficient environment, thus the sulfates, as shown in Fig. 3a, are predicted to exist in the aerosol phase in the form of SO_4^{2-}. On the other hand, in case (b) the environment is sulfate rich, thus about 25% of the initial sulfuric acid is predicted to be in the aerosol phase in the form of HSO_4^-, while the rest as SO_4^{2-}. The increased concentration of H_2SO_4 in the aerosol phase in the latter case (Fig. 3b) causes a sharp decrease in both the NO_3^- and Cl^- concentrations in the particulate phase. In both cases the OH^- concentration is predicted to be negligible.

The next example demonstrates the dependence of the composition of the

aerosol phase on the NaCl size distribution. In this set of runs the system was assumed to consist of 10 μg m^{-3} NaCl, 10 μg m^{-3} H_2SO_4, 0 μg m^{-3} HCl, 5 μg m^{-3} NH_3 and 5 μg m^{-3} HNO_3, while the ambient temperature was assumed to be 298 K and the relative humidity 40%. The aerosol was assumed to consist of two size sections, one fine, 0.02-0.1 μm, and one coarse, 0.1-10.0 μm, with 90% of the H_2SO_4 in the fine section and 10% in the coarse section. Figure 4 shows the predicted composition in the aerosol phase, as a function of the fraction of the total NaCl lying in the coarse section. As the fraction of NaCl in the coarse section increases, less NaCl is available in the fine section to react with the abudant H_2SO_4, thus reducing the produced Na_2SO_4. The inverse behavior is observed for $(NH_4)_2SO_4$. The remaining H_2SO_4 (after NaCl has been completely consumed in the fine section) reacts with ammonia, thus increasing the ammonium sulfate concentration.

In contrast to the Na_2SO_4 and $(NH_4)_2SO_4$, the behavior of which is controlled by reactions in the fine section, the concentration of $NaNO_3$ and NaCl is controlled by reactions in the coarse section. As NaCl increases in the coarse particles, part of it reacts completely with the H_2SO_4 in this section. The rest of it reacts directly with the HNO_3, until the equilibrium of the reaction

$$NaCl_{(s)} + HNO_{3(g)} \rightleftharpoons NaNO_{3(s)} + HCl_{(g)}$$

is established. One should note that no NH_4NO_3 is predicted to be formed. The total amount of ammonium is predicted to lie in the fine section as ammonium sulfate, while the total amounts of nitrate and chloride are predicted to lie in the coarse section, in the form of NaCl and $NaNO_3$.

SIMULATION OF AEROSOL COMPOSITION IN THE SOUTH COAST AIR BASIN OF CALIFORNIA

We will now apply our model to predict the behavior of the composition of inorganic aerosol in the South Coast Air Basin of California and we will compare its predictions to observed values.

Measurements in the Los Angeles area during 1972 (Ho et al; 1974) showed that the liquid water content of atmospheric aerosols accounts for 10-40% of the total particulate mass, for relative humidities from 50-70%, while for RH above 70% the liquid water fraction was increased significantly. Using typical values observed in the same area we seek to predict the quantity of aerosol water. Figure 5 shows the measured water fraction in the aerosol phase in the Los Angeles area during 1972 (Ho et al, 1974), as well as the predicted water fraction for 1 and 10 μg m^{-3} NH_3, as a function of the relative humidity. The rest of the input concentrations in the model were assumed to be 5 μg m^{-3} NaCl, 20 μg m^{-3} HNO_3, 10 μg m^{-3} H_2SO_4 and 0 μg m^{-3} HCl, while the ambient temperature is assumed to be 298 K. Such conditions were observed in Los Angeles, California in August 1982 (Russell and Cass, 1984). The aerosol was assumed to consist of two size sections with 90% of the H_2SO_4 and 10% of the NaCl in the fine section.

Figure 5 shows the predicted water mass fraction for both the cases. As is shown, for high relative humidities, higher than 62%, the predictions of both the runs match the observed water fraction in Los Angeles in 1972 within the uncertainty of the measurements. An important observation from Fig. 5 is that for high relative humidities the water fraction in the aerosol phase, in spite of being

very sensitive to the relative humidity, is relatively robust to changes of the concentration of the inorganic condensible species. Physically this behavior can be explained by the fact that, since the aqueous phase is thermodynamically favored at high humidities, the more sulfate, nitrate, ammonium and chloride that condense in the aerosol phase the more water condenses to achieve the thermodynamic equilibrium, given the ambient temperature and relative humidity.

Below 62% RH the behavior between the two aerosols is quite different. The aerosol that corresponds to 10 μg m^{-3} of NH_3 shows a clear deliquesence behavior at 62%, which is the deliquesence relative humidity of NH_4NO_3, the lowest deliquesence point in the sulfate poor case. In contrast the aerosol that corresponds to 1 μg m^{-3} of NH_3 shows the existence of water even at very low relative humidities, indicating hygroscopic behavior. This behavior can be explained with the help of Figure 6, which presents the size composition distribution of the aerosol at 36% RH in the case of 1 μg m^{-3} of NH_3. As shown in this figure the assumed small quantity of atmospheric NH_3 is not enough to neutralize the sulfuric acid that is assumed to be in the fine section. Thus, the thermodynamic equilibrium predicts that $H_2SO_{4(l)}$ should exist, which being hygroscopic attracts water even at very low relative humidities. The coarse section, since it is completely neutralized by the NaCl reactions with the acids is predicted to be dry. Thus, in this case, we have the interesting behavior of dry coarse and wet fine particles. Note that no deliquesent behavior is predicted, which may be a possible explanation of the lack of deliquesent behavior of atmospheric aerosols observed in many parts of the USA (Covert et al, 1972).

The large differences in the water content at low relative humidities, due to

deliquesence and hydroscopic phenomena, indicate that the aerosol water fraction, in contrast to high relative humidities, is very sensitive to the ambient concentrations of the rest of the species.

Figure 7 shows the predicted aerosol composition and physical state as a function of the relative humidity for 10 μg m^{-3} initial NH_3. At low relative humidities, below 62%, the aerosol is predicted to consist of a mixture of solid Na_2SO_4, $(NH_4)_2SO_4$, NH_4NO_3 and $NaNO_3$. Above 62% RH, the critical humidity for NH_4NO_3, the ammonium nitrate is completely dissolved. The condensed water is predicted to be enough to cause the complete dissolution of the rest of the salts. Thus, above this RH the particle is predicted to be an aqueous solution of Na^+, NH_4^+, NO_3^-, Cl^-, and SO_4^{2-}, despite the fact that the deliquesence point of most of the rest of the thermodynamically favored salts is about 80% RH.

A field study took place throughout the California's South Coast Air Basin on August 30-31, 1982 (Russell and Cass, 1984; Hildelmann et al, 1984). During that study aerosol particles were collected and the amount of ionic material in the aerosol phase was determined. Thus 4-hr and 2-hr average data for Aug. 30 and Aug. 31, respectively, are available for inorganic aerosol material, as well as NH_3, HNO_3 and ambient meteorological conditions. Unfortunately neither HCl in the gas phase nor liquid H_2O was measured. We simulated the aerosol concentrations observed at Long Beach, California throughout the 48-hrs that measured data exist.

The Long Beach prediction is a difficult test for aerosol equilibrium models, because during those 48-hrs the air mass stagnated for most of the day in an area of high NO_x and SO_2 emissions, resulting in high concentrations of sulfate and

nitrate aerosols, despite the high ambient temperature, which, thermodynamically, does not favor aerosol formation (Russell et al; 1982, Russell and Cass; 1984).

Air masses from the Pacific Ocean cross the Long Beach coastline, carrying coarse aerosol, rich in sea salt, inland. Sulfur dioxide is produced in that area, the photooxidation of which produces H_2SO_4 that, by homogeneous nucleation and condensation, can be transferred into the aerosol phase. Hence it is reasonable to consider that most of the NaCl at Long Beach lies in the coarse particles, while the H_2SO_4 lies in the fine ones. This assumption is supported by measurements of the aerosol size-composition distribution in many locations in California (Wall et al, 1987). Thus we consider two size sections, assuming that 90% of the aerosol sodium exists in the coarse section, while 90% of the aerosol sulfate lies in the fine section.

Because no HCl data are available we assumed that all the sodium in the aerosol phase was initially in the form of NaCl and that NaCl was the only possible source of HCl. Whenever other cations, such as Ca^{2+}, Mg^{2+} and K^+, were present, their concentrations were reduced to equivalent sodium. Inputs to our calculation were the total measured H_2SO_4 and equivalent NaCl, distributed as described above, the total measured nitrates (i.e. $HNO_3 + NO_3^-$) and the total measured ammonium (i.e. $NH_4^+ + NH_3$), as well as the measured ambient temperature and relative humidity. Predicted were the total ammonium, chloride and nitrate concentrations in the aerosol phase, as well as the NH_3, HNO_3 and HCl in the gas phase at thermodynamic equilibrium. Also the water content and the thermodynamically favorable species for both the fine and coarse particles were predicted.

Figures 8, 9 and 10 show the predicted and observed total concentrations of nitrates, ammonium, and chlorides in the aerosol phase, respectively, for the Aug. 30-31, 1982 period at Long Beach, California. As shown in Fig. 8, we predict the nitrates in the aerosol phase within the uncertainty of the measurements throughout the 48-hr period, except for the peak between 800 and 1200 PDT of Aug. 31, 1982. For this time period the model predicts that the concentration of nitrates at Long Beach reaches a maximum, but the predicted nitrate concentration is lower than the mean observed value.

Fig. 9 shows the predicted and observed NH_4^+ for the same period of time. Despite the small consistent overprediction, the behavior of the ammonium concentration as a function of time is predicted. Chlorides, as shown in Fig. 10, are predicted quite well for many of the cases. For the others there is overprediction of the chloride concentrations, which is probably due to the lack of HCl data and our assumption that all the sodium in the aerosol phase was initially in the form of NaCl.

Figure 11 shows the predicted distribution of the aerosol water between the fine and the coarse aerosol at 0-200 PDT of Aug. 31, 1982. Twice as much water is predicted to be in the large particles than in the small ones. Due to the high relative humidity, 81%, the aerosol is predicted to be an aqueous solution of ionic material. Figure 12 shows the distribution of the various ions between the two size sections, for the same case. Most of the Cl^- and NO_3^- is predicted to be in the coarse section, where most of the sodium exists, while most of the NH_4^+ is predicted to lie in the fine section, directly associated with the abudance of sulfate in that section.

Exactly the same behavior is noted in Fig. 13, which shows the predicted distribution between the two size sections, at Long Beach, California for the period 1400-1600 PDT of Aug. 31, 1982. Because the relative humidity was only 43%, the aerosol is predicted to be a mixture of solid salts. Note that the aerosol nitrate and chloride are predicted to lie in the large particles, as $NaNO_3$ and NaCl, respectively, and that the ammonium is, again, predicted to be in the small size section, as $(NH_4)_2SO_4$, while no NH_4NO_3 is predicted to be formed during that 2-hr period at Long Beach, California.

CONCLUSIONS

An equilibrium model of the ammonium/ chloride/ nitrate/ sodium/ sulfate/ water aerosol system has been presented. Given the total quantities of HNO_3, NH_3 and HCl in the gas phase, as well as the distribution of NaCl and H_2SO_4 in the aerosol phase, the chemical composition-distribution and physical state of the aerosol is calculated, for given temperature and relative humidity.

Using this model, we have shown that the observed existence, in Los-Angeles, of liquid water in the aerosol phase at low relative humidities can be explained by the means of thermodynamic equilibrium. The model also successfully predicted the amount of the aerosol NO_3^-, NH_4^+ and Cl^- existing at Long Beach, California during the episode of August 30-31, 1982.

ACKNOWLEDGEMENT

This work was supported by the State of California Air Resources Board Agreement A4-146-32.

REFERENCES

Bassett M.E. and Seinfeld J.H. (1983) Atmospheric equilibrium model of sulfate and nitrate aerosol. Atmospheric Environment 17, 2237-2252.

Bassett M.E. and Seinfeld J.H. (1984) Atmospheric equilibrium model of sulfate and nitrate aerosol-II. Particle size analysis. Atmospheric Environment 18, 1163-1170.

Bromley L. A. (1973) Thermodynamic properties of strong electrolytes in aqueous solutions. AIChE J., 19, 313-320.

Cohen M. D., Flagan R. C. and Seinfeld J. H. (1987a). Studies of concentrated electrolyte solutions using the electrodynamic balance. I. Water activities for single-electrolyte solutions. J. Phys. Chem. (submitted for publication)

Cohen M. D., Flagan R. C. and Seinfeld J. H. (1987b). Studies of concentrated electrolyte solutions using the electrodynamic balance. II. Water activities for mixed-electrolyte solutions. J. Phys. Chem. (submitted for publication)

Covert D. S., Charlson R. J. and Ahlquist N. C. (1972) A study of the relationship of chemical composition and humidity of light scattering by aerosols. J. Appl. Meteor., 11, 968-976.

Denbigh K. (1981) The principles of chemical equilibrium. Fourth Ed. Cambridge University Press, Cambridge.

Jacob D. J., Waldman J. M., Munger J. W. and Hoffmann M. R. (1986) The H_2SO_4-HNO_3-NH_3 system at high humidities and in fogs 2. Comparison of field data with thermodynamic calculations. J. Geophys. Res., 91, 1089-1096.

Jacob D. J., Waldman J. M., Munger J. W. and Hoffmann M. R. (1985) Chemical composition of fogwater collected along the California coast. Environ. Sci. Technol., 19, 730-736.

Hänel G. (1970) The size of atmospheric aerosol particles as a function of relative humidity. Beitr. Phys. Atmos., 43, 119-132.

Hidy G. M., Appel B. R., Charlson R. J., Clark W. E., Friedlander S. K., Hutchison D. H., Smith J. B., Suder J., Wesolowski J. J. and Whitby K. J. (1975). Summary of the California aerosol characterization experiment. J. Air Pollut. Control Ass. 25, 1106-1114.

Hildelmann L. M., Russell A.G. and Cass G.R. (1984) Ammonia and nitric acid concentrations in equilibrium with atmospheric aerosols: Experiment vs. theory. Atmospheric Environment 18, 1737-1750.

Hitchcock D. R., Spiller L. L., and Wilson, W. E. (1980) Sulfuric acid aerosols and HCl release in coastal atmosperes: Evidence of rapid formation of sulfuric acid particulates. Atmospheric Environment 14, 165-182.

Ho W., Hidy G. M., and Govan R. M. (1974) Microwave Measurements of the Liquid Water Content of Atmospheric Aerosols. J. Appl. Meteor., 13, 871-879.

John W., Wall S. M. and Ondo J. L. (1985) Dry acid deposition on materials and vegetation: Conentrations in ambient air. Final report prepared for the California Air Resources Board. Interagency Agreement A1-160-32.

John W., Wall S. M. and Ondo J. L. (1987) A new method for nitric acid and nitrate aerosol measurement using the dichotomous sampler. Atmospheric Environment XX, XXXX-XXXX.

Orsini C. Q., Tabacnicks M. H., Artaxo P., Andrade, M. F. and Kerr A. S. (1986) Characteristics of fine and coarse particles of natural and urban aerosols in Brazil. Atmospheric Environment 20, 2259-2269.

Pilinis C., Seinfeld J.H. and Seigneur C. (1987) Mathematical modeling of

the dynamics of multicomponent atmospheric aerosols. Atmospheric Environment 21, 943-955.

Pitzer K. S. and Mayorga G. (1973) Thermodynamics of electrolytes. II. Activity and Osmotic coefficients for strong electrolytes with one or both ions univalent. J. Phys. Chem., 77, 2300-2308.

Robinson R. A. and Stokes R. H. (1965). Electrolyte Solutions. Second Ed. Butterworth and CO., London.

Russell A.G., McRae G. J. and Cass G. R. (1983) Mathematical modeling of the formation and transport of ammonium nitrate aerosol. Atmospheric Environment 17, 949-964.

Russell A.G. and Cass G. R. (1984) Aquisition of regional air quality model validation data for nitrate, sulfate, ammonium ions, and their precursors. Atmospheric Environment 18, 1815-1827.

Sangster J. and Lenzi F. (1974) On the choice of methods for the prediction of the water activity and activity coefficient for multicomponent aqueous solutions. Can. J. of Chem. Eng., 52, 392-396.

Saxena P. and Peterson T. W. (1981) Thermodynamics of multicomponent electrolytic aerosols. J. Colloid Interface Sci., 79, 496-510.

Saxena P., Seigneur C. and Peterson T. W. (1983) Modeling of multiphase atmospheric aerosols. Atmospheric Environment 17, 1315-1329.

Saxena P., Hudischewskyj A. B., Seigneur C. and Seinfeld J. H. (1986) A comparative study of equilibrium approaches to the chemical characterization of secondary aerosols. Atmospheric Environment 20, 1471-1483

Seigneur C. and Saxena P. (1984) A study of atmospheric acid formation in

different environments. Atmospheric Environment 18, 2109-2124.

Seinfeld J. H. (1986) Atmospheric Chemistry and Physics of Air Pollution, John Wiley, New York.

Stelson A. W., Friedlander S. K. and Seinfeld J. H. (1979) A note on the equilibrium relationship between ammonia and nitric acid and particulate ammonium nitrate. Atmospheric Environment 13, 369-371.

Stelson A. W. and Seinfeld J. H. (1982a) Relative humidity and temperature dependence of the ammonium nitrate dissociation constant. Atmospheric Environment 16, 983-992.

Stelson A. W. and Seinfeld J. H. (1982b) Relative humidity and pH dependence of the vapor pressure of ammonium nitrate-nitric acid solutions at 25° C. Atmospheric Environment 16, 993-1000.

Stelson A. W. and Seinfeld J. H. (1982c) Thermodynamic prediction of the water activity, NH_4NO_3 dissociation constant, density and refractive index for the NH_4NO_3-$(NH_4)_2SO_4$-H_2O system at 25° C. Atmospheric Environment 16, 2507-2514.

Wagman D. D., Evans W. H., Parker V. B., Harlow I., Baily S. M. and Schumm R. H. (1968). Selected values of chemical thermodynamic properties; tables for the first thirty-four elements in the standar order of arrangement. NBS Technical note 270-3.

Wall S. M., John W. and Ondo J. L. (1987) Measurements of aerosol size distributions for nitrate and major ionic species. Atmospheric Environment XX, XXXX-XXXX.

Winkler P. (1973) The growth of atmospheric aerosol particles as a function

of the relative humidity-II. An improved concept of mixed nuclei. J. Aerosol Sci. 4, 373-387.

Table 1. Chemical reactions occuring in the NaCl-HCl-H_2SO_4-NH_3-HNO_3-H_2O system.

Reaction	Equilibrium Constant
$NaCl_{(s)} + HNO_{3(g)} \rightleftharpoons NaNO_{3(s)} + HCl_{(g)}$	$3.00exp\left[5.50\left(\frac{T_o}{T}-1\right)-2.180\left(1+ln(\frac{T_o}{T})-\frac{T_o}{T}\right)\right]$
$NH_{3(g)} + HNO_{3(g)} \rightleftharpoons NH_4^+ + NO_3^-$	$3.99\times10^{17}exp\left[64.7\left(\frac{T_o}{T}-1\right)+11.51\left(1+ln(\frac{T_o}{T})-\frac{T_o}{T}\right)\right]$ mol^2 Kg^{-2} atm^{-2}
$HCl_{(g)} \rightleftharpoons H^+ + Cl^-$	$2.03\times10^{6}exp\left[30.21\left(\frac{T_o}{T}-1\right)+19.91\left(1+ln(\frac{T_o}{T})-\frac{T_o}{T}\right)\right]$ mol^2 Kg^{-2} atm^{-1}
$NH_{3(g)} + HCl_{(g)} \rightleftharpoons NH_4^+ + Cl^-$	$2.12\times10^{17}exp\left[65.08\left(\frac{T_o}{T}-1\right)+14.51\left(1+ln(\frac{T_o}{T})-\frac{T_o}{T}\right)\right]$ mol^2 Kg^{-2} atm^{-2}
$Na_2SO_{4(s)} \rightleftharpoons 2Na^+ + SO_4^{2-}$	$0.4805exp\left[0.98\left(\frac{T_o}{T}-1\right)+39.57\left(1+ln(\frac{T_o}{T})-\frac{T_o}{T}\right)\right]$ mol^3 Kg^{-3}
$(NH_4)_2SO_{4(s)} \rightleftharpoons 2NH_4^+ + SO_4^{2-}$	$1.425exp\left[-2.65\left(\frac{T_o}{T}-1\right)+38.55\left(1+ln(\frac{T_o}{T})-\frac{T_o}{T}\right)\right]$ mol^3 Kg^{-3}
$HSO_4^- \rightleftharpoons H^+ + SO_4^{2-}$	$1.031\times10^{-2}exp\left[7.59\left(\frac{T_o}{T}-1\right)+18.83\left(1+ln(\frac{T_o}{T})-\frac{T_o}{T}\right)\right]$ mol Kg^{-1}
$HNO_{3(g)} \rightleftharpoons H^+ + NO_3^-$	$3.638\times10^{6}exp\left[20.47\left(\frac{T_o}{T}-1\right)+16.84\left(1+ln(\frac{T_o}{T})-\frac{T_o}{T}\right)\right]$ mol^2 Kg^{-2} atm^{-1}
$NH_4Cl_{(s)} \rightleftharpoons NH_{3(g)} + HCl_{(g)}$	$1.039\times10^{-16}exp\left[-71.04\left(\frac{T_o}{T}-1\right)+2.40\left(1+ln(\frac{T_o}{T})-\frac{T_o}{T}\right)\right]$ atm^2
$NH_{3(g)} + HNO_{3(g)} \rightleftharpoons NH_4NO_{3(s)}$	$3.340\times10^{16}exp\left[75.11\left(\frac{T_o}{T}-1\right)-13.40\left(1+ln(\frac{T_o}{T})-\frac{T_o}{T}\right)\right]$ atm^{-2}
$NaNO_{3(s)} \rightleftharpoons Na^+ + NO_3^-$	$11.971exp\left[-8.22\left(\frac{T_o}{T}-1\right)+16.01\left(1+ln(\frac{T_o}{T})-\frac{T_o}{T}\right)\right]$ mol^2 Kg^{-2}
$NaCl_{(s)} \rightleftharpoons Na^+ + Cl^-$	$37.743exp\left[-1.57\left(\frac{T_o}{T}-1\right)+16.89\left(1+ln(\frac{T_o}{T})-\frac{T_o}{T}\right)\right]$ mol^2 Kg^{-2}
$NaHSO_{4(s)} \rightleftharpoons Na^+ + HSO_4^-$	$2.44\times10^{4}exp\left[0.79\left(\frac{T_o}{T}-1\right)+4.53\left(1+ln(\frac{T_o}{T})-\frac{T_o}{T}\right)\right]$ mol^2 Kg^{-2}

Table 2. Relative humidities of deliquesence of the nine possible solid compounds.

Species	Deliquesence RH
NaCl	76.0
Na_2SO_4	93.0
$NaHSO_4$	52.0
$NaNO_3$	74.0
NH_4Cl	80.0
$(NH_4)_2SO_4$	80.0
$(NH_4)_3H(SO_4)_2$	69.0
NH_4HSO_4	40.0
NH_4NO_3	62.0

Table 3. Aerosol chemical composition as a function of the ambient relative humidity for the sulfate deficient case.

RH	SPECIES
100	
	Na^+, Cl^-, SO_4^{2-}, NH_4^+, NO_3^-, H_2O
93	
	$Na_2SO_{4(s)}$, H_2O
	Na^+, Cl^-, SO_4^{2-}, NH_4^+, NO_3^-
80	
	$Na_2SO_{4(s)}$, $NH_4Cl_{(s)}$, $(NH_4)_2SO_{4(s)}$, H_2O
	Na^+, Cl^-, SO_4^{2-}, NH_4^+, NO_3^-
76	
	$Na_2SO_{4(s)}$, $NH_4Cl_{(s)}$, $(NH_4)_2SO_{4(s)}$,
	$NaCl_{(s)}$, H_2O
	Na^+, Cl^-, SO_4^{2-}, NH_4^+, NO_3^-
74	
	$Na_2SO_{4(s)}$, $NH_4Cl_{(s)}$, $(NH_4)_2SO_{4(s)}$,
	$NaNO_{3(s)}$, $NaCl_{(s)}$, H_2O
	Na^+, Cl^-, SO_4^{2-}, NH_4^+, NO_3^-
62	
	$Na_2SO_{4(s)}$, $NH_4Cl_{(s)}$, $(NH_4)_2SO_{4(s)}$,
	$NH_4NO_{3(s)}$, $NaNO_{3(s)}$, $NaCl_{(s)}$
0	

Table 4. Aerosol chemical composition as a function of the ambient relative humidity for the sulfate rich case.

	$1 \leq R_{H_2SO_4} < 2$	$0 \leq R_{H_2SO_4} < 1$
RH	SPECIES	SPECIES
100		
	Na^+, Cl^-, SO_4^{2-}, NH_4^+, NO_3^-, H_2O	
	H^+, $HNO_{3(l)}$, HSO_4^-	
93		
	$Na_2SO_{4(s)}$, H_2O	
	Na^+, Cl^-, SO_4^{2-}, NH_4^+, NO_3^-	
	H^+, $HNO_{3(l)}$, HSO_4^-	
80		
	$Na_2SO_{4(s)}$, $(NH_4)_2SO_{4(s)}$, H_2O	H^+, $HNO_{3(l)}$, HSO_4^-, $H_2SO_{4(l)}$
	Na^+, Cl^-, SO_4^{2-}, NH_4^+, NO_3^-	NO_3^-, Na^+, Cl^-, NH_4^+, H_2O
	H^+, $HNO_{3(l)}$, HSO_4^-	
69		
	$Na_2SO_{4(s)}$, $(NH_4)_2SO_{4(s)}$, $(NH_4)_3H(SO_4)_{2(s)}$	
	Na^+, Cl^-, SO_4^{2-}, NH_4^+, NO_3^-	
	H^+, $HNO_{3(l)}$, HSO_4^-, H_2O	
52		
	$Na_2SO_{4(s)}$, $(NH_4)_2SO_{4(s)}$, $(NH_4)_3H(SO_4)_{2(s)}$	
	$NaHSO_{4(s)}$, H_2O	$NaHSO_{4(s)}$, H_2O
	Na^+, Cl^-, SO_4^{2-}, NH_4^+, NO_3^-	Na^+, Cl^-, NH_4^+, NO_3^-
	H^+, $HNO_{3(l)}$, HSO_4^-	H^+, $HNO_{3(l)}$, HSO_4^-, $H_2SO_{4(l)}$
40		
	$Na_2SO_{4(s)}$, $(NH_4)_2SO_{4(s)}$, $(NH_4)_3H(SO_4)_{2(s)}$,	$NaHSO_{4(s)}$, H_2O, Na^+, Cl^-, NH_4^+, NO_3^-
	$NaHSO_{4(s)}$, $NH_4HSO_{4(s)}$,	$NH_4HSO_{4(s)}$, H^+, HSO_4^-, $HNO_{3(l)}$, $H_2SO_{4(l)}$
0		

Table 5. Coefficients of the polynomial fit of the binary solution water activity, $a_w = \sum_{i=0}^{6} a_i m^i$.

Species	a_0	a_1	a_2	a_3	a_4	a_5	a_6
$NaNO_3$	0.9988	-2.0947×10^{-2}	1.9010×10^{-4}	2.8154×10^{-5}	-0.1350×10^{-7}	0.0	0.0
$NaHSO_4$	1.0614	-0.1014	1.5790×10^{-2}	-1.9501×10^{-3}	9.5147×10^{-5}	-1.5473×10^{-6}	0.0
NaCl	1.0084	-4.9390×10^{-2}	8.8880×10^{-3}	-2.1570×10^{-3}	1.6170×10^{-4}	-1.9900×10^{-6}	-1.1420×10^{-7}
Na_2SO_4	1.0052	-0.4840×10^{-2}	3.5190×10^{-2}	-1.3100×10^{-2}	1.0250×10^{-3}	-1.2240×10^{-4}	2.8700×10^{-6}
$(NH_4)_2SO_4$	0.9968	-2.9690×10^{-2}	1.7350×10^{-5}	-3.2530×10^{-4}	3.5710×10^{-6}	-0.7870×10^{-7}	0.0
NH_4Cl	0.9908	-2.0110×10^{-2}	-1.5990×10^{-3}	1.3550×10^{-4}	-2.3170×10^{-6}	-1.1130×10^{-8}	0.0
NH_4NO_3	1.0053	-2.4091×10^{-2}	4.4088×10^{-4}	1.6453×10^{-5}	-3.8040×10^{-7}	-4.7608×10^{-8}	1.3753×10^{-9}
NH_4HSO_4	1.0261	-4.9766×10^{-2}	3.2757×10^{-3}	-2.4477×10^{-4}	1.0700×10^{-5}	-1.8329×10^{-7}	0.0
$(NH_4)_3H(SO_4)_2$	1.0088	-5.3730×10^{-2}	1.4201×10^{-3}	-9.2484×10^{-4}	2.2790×10^{-4}	-1.5445×10^{-6}	0.0
H_2SO_4	1.0175	-3.2120×10^{-2}	-9.5203×10^{-3}	8.7831×10^{-4}	-2.8025×10^{-5}	3.0897×10^{-7}	0.0
HCl	0.9992	-3.0929×10^{-2}	-4.0896×10^{-3}	5.3711×10^{-5}	2.2489×10^{-5}	-7.7602×10^{-7}	0.0
HNO_3	0.9988	-3.0466×10^{-2}	-2.8124×10^{-3}	-3.8709×10^{-7}	1.0932×10^{-5}	-2.0014×10^{-7}	0.0

Table 6: Parameters of Pitzer's method.

Species	$\beta_{12}^{(0)}$	$\beta_{12}^{(1)}$	$\frac{2}{3}C_{12}^{\gamma}$
NaCl	0.10820	0.03127	-0.002469
Na_2SO_4	0.08610	0.13037	-0.003104
$NaNO_3$	0.00680	0.17830	-0.000720
$NaHSO_4$	0.35262	1.56403	-0.009978
NH_4Cl	0.04568	0.20431	-0.001731
$(NH_4)_2SO_4$	0.04763	0.44459	-0.001311
NH_4NO_3	-0.01540	0.11200	-0.000030
NH_4HSO_4	0.04494	0.23594	-0.002920
(H^+, HSO_4^-)	0.25713	0.35308	-0.002830
$(2H^+, SO_4^{2-})$	-0.09330	0.32381	0.021162
HNO_3	0.11190	0.32060	0.001000
HCl	0.17750	0.29450	0.000800

Table 7

SO_4^{2-}, NO_3^-, NH_4^+ and H_2O concentrations

obtained by the aerosol equilibrium models SEQUILIB, EQUIL and MARS

for T=298 K, 10 $\mu g\ m^{-3}$ H_2SO_4, 10 $\mu g\ m^{-3}$ NH_3 and 30 $\mu g\ m^{-3}$ HNO_3.

RH	SEQUILIB				EQUIL				MARS			
	SO_4^{2-}	NO_3^-	NH_4^+	H_2O	SO_4^{2-}	NO_3^-	NH_4^+	H_2O	SO_4^{2-}	NO_3^-	NH_4^+	H_2O
51	10.0	12.9	7.4	0.0	10.0	14.0	7.7	0.0	10.0	13.0	7.4	0.0
56	10.0	12.9	7.4	0.0	10.0	14.0	7.7	0.0	10.0	13.0	7.4	0.0
61	10.0	12.9	7.4	0.0	10.0	14.0	7.7	0.0	10.0	13.0	7.4	0.0
66	10.0	14.0	7.8	19.0	9.90	15.1	8.1	5.3	10.0	0.00	3.7	0.0
71	10.0	15.5	8.2	26.0	9.70	16.9	8.6	28.8	10.0	15.6	8.2	25.7
76	10.0	16.8	8.6	35.1	9.70	18.0	8.9	36.7	10.0	17.2	8.7	35.9
81	10.0	18.3	9.0	49.1	9.70	19.1	9.2	49.5	10.0	18.6	9.1	50.5
86	10.0	19.7	9.4	73.1	9.70	20.3	9.5	73.8	10.0	19.1	9.5	75.5
91	10.0	21.2	9.8	124.0	9.50	21.9	9.9	131.0	10.0	21.4	9.9	131.9

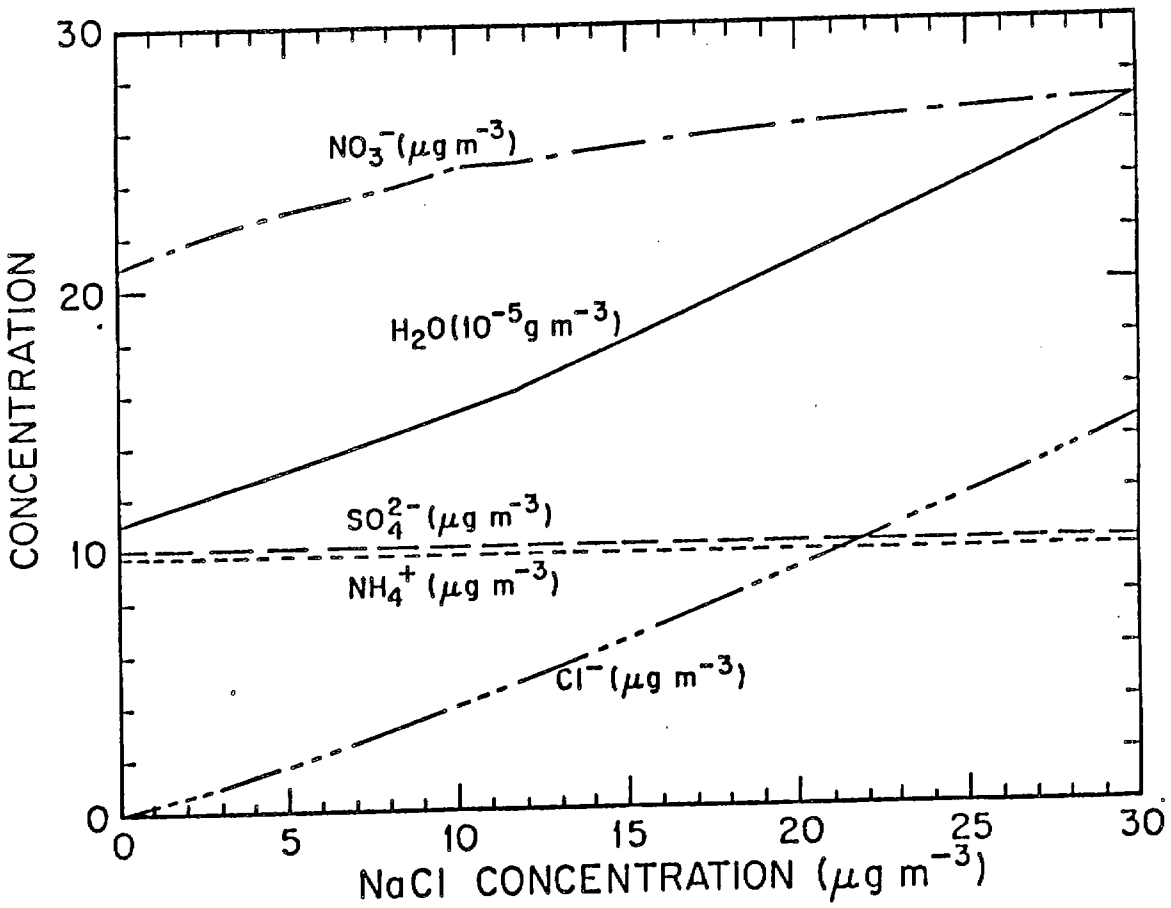

Fig. 1 Aerosol composition as a function of the NaCl concentration for 90% relative humidity. The conditions are 10 $\mu g\ m^{-3}$ H_2SO_4, 0 $\mu g\ m^{-3}$ HCl, 10 $\mu g\ m^{-3}$ NH_3 and 30 $\mu g\ m^{-3}$ HNO_3, ambient temperature is 298 K.

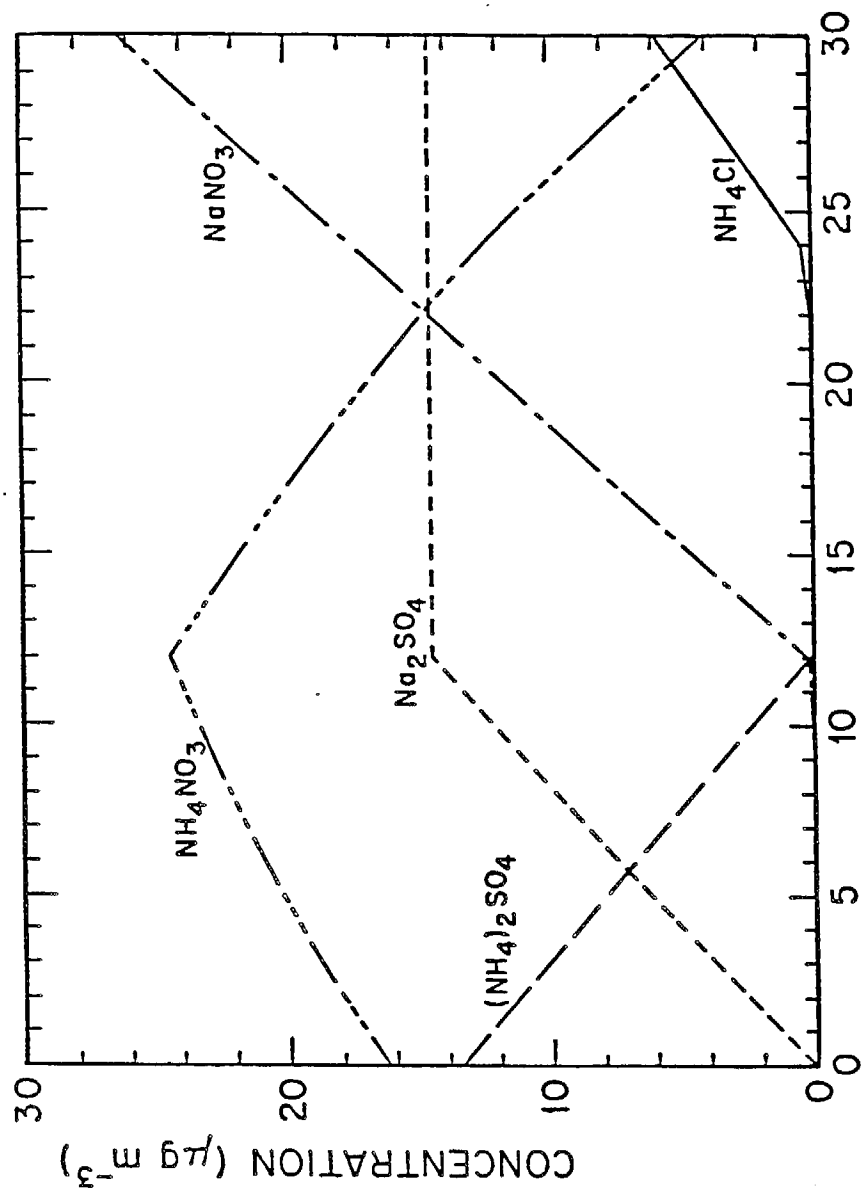

Fig. 2 Aerosol composition as a function of the NaCl concentration for 40% relative humidity. The conditions are 10 $\mu g\ m^{-3}$ H_2SO_4, 0 $\mu g\ m^{-3}$ HCl, 10 $\mu g\ m^{-3}$ NH_3 and 30 $\mu g\ m^{-3}$ HNO_3, ambient temperature is 298 K.

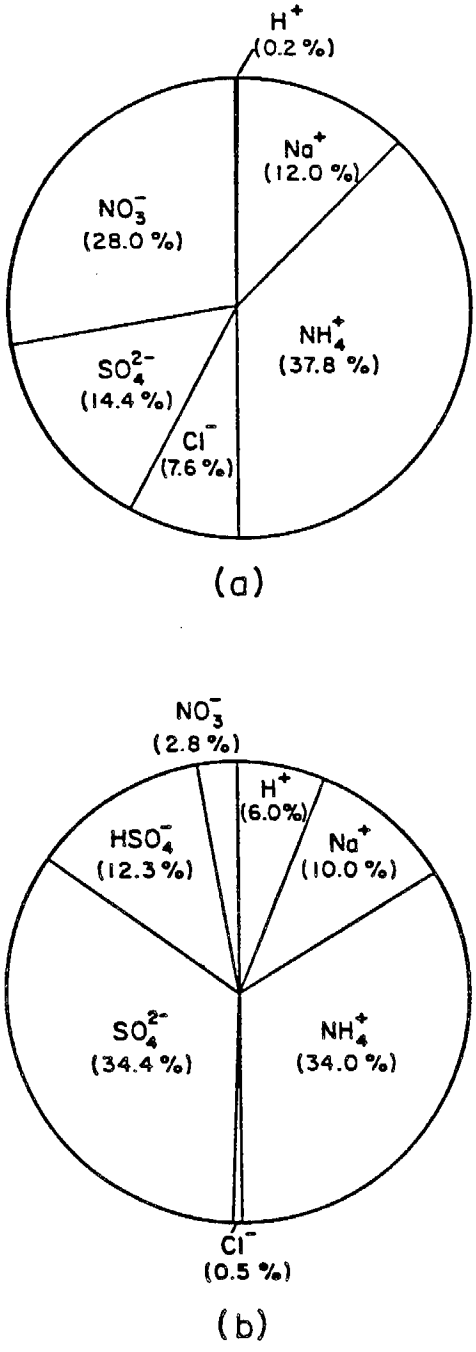

Fig. 3 Aerosol composition by equivalents (%). Case (a) corresponds to 10 μg m^{-3} H_2SO_4, while case (b) to 50 μg m^{-3} H_2SO_4. The other conditions are 15 μg m^{-3} NaCl, 0 μg m^{-3} HCl, 10 μg m^{-3} NH_3 and 30 μg m^{-3} HNO_3, ambient temperature is 298 K and ambient RH 90%.

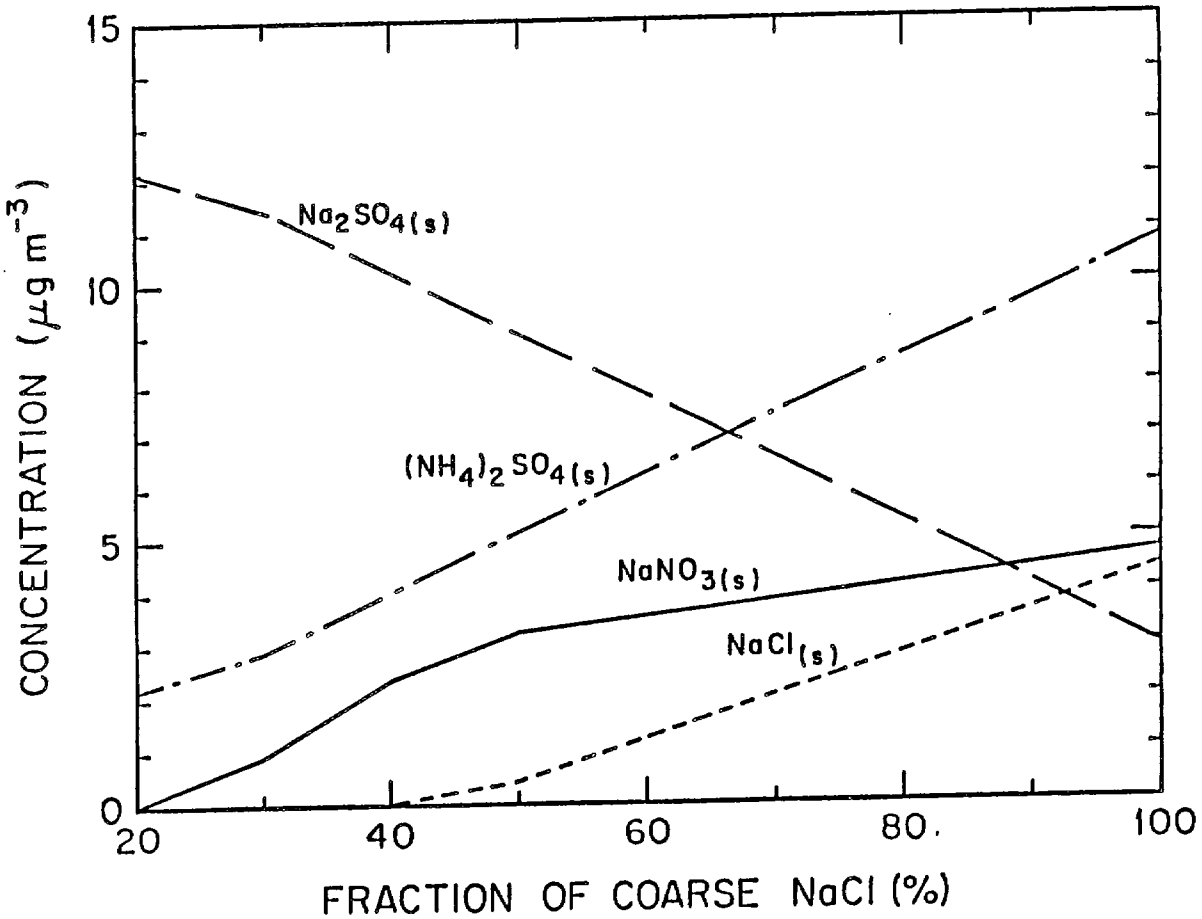

Fig. 4 Aerosol composition as a function of the fraction of NaCl in the coarse section of a two size section aerosol. The conditions are 10 μg m^{-3} NaCl, 10 μg m^{-3} H_2SO_4, 0 μg m^{-3} HCl, 5 μg m^{-3} NH_3 and 5 μg m^{-3} HNO_3, ambient temperature is 298 K and relative humidity is 40%.

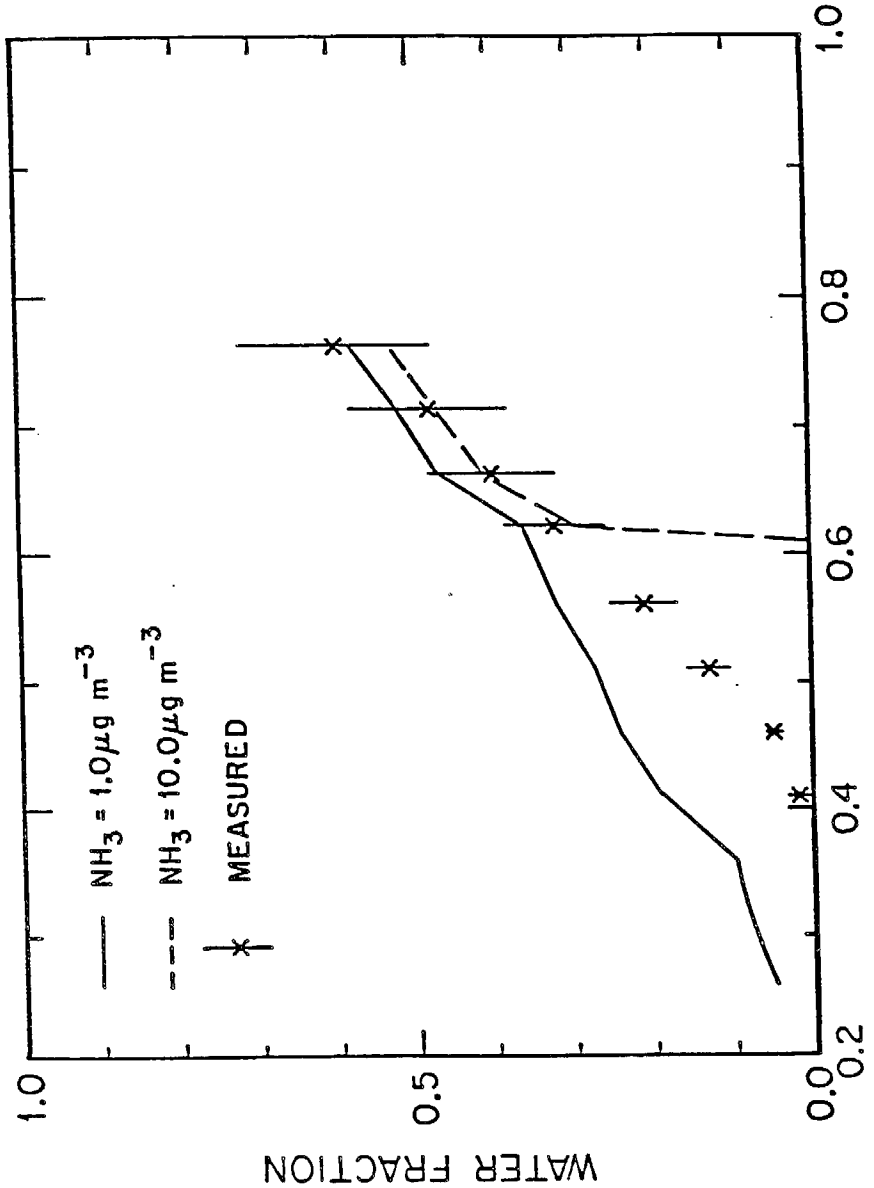

Fig. 5 Predicted water mass fraction as a function of the relative humidity for 1 and 10 $\mu g\ m^{-3}$ NH_3. The other conditions are 5 $\mu g\ m^{-3}$ NaCl, 20 $\mu g\ m^{-3}$ HNO_3, 10 $\mu g\ m^{-3}$ H_2SO_4 and 0 $\mu g\ m^{-3}$ HCl. The error bars correspond to observed values in Los Angeles, CA. (Ho et al, 1974)

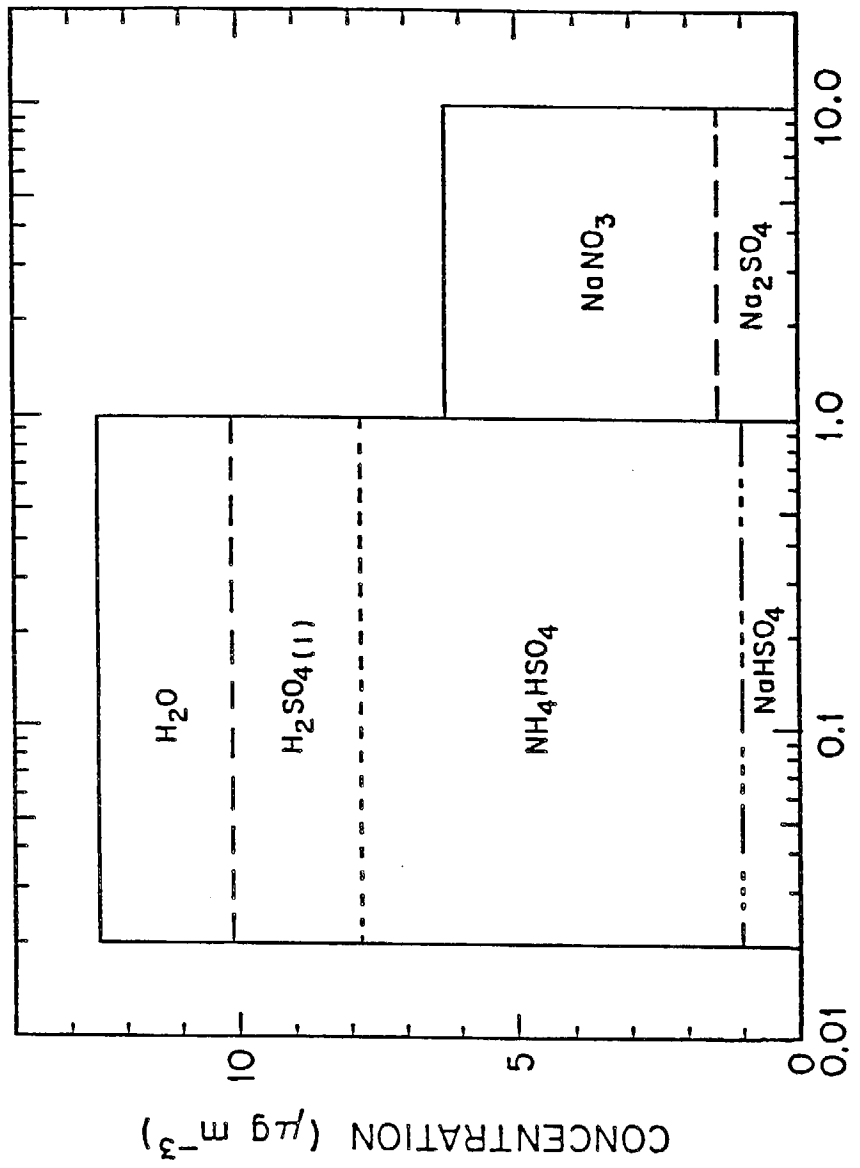

Fig. 6 Predicted size-composition distribution for 1 $\mu g\ m^{-3}$ NH_3. The other conditions are 5 $\mu g\ m^{-3}$ NaCl, 20 $\mu g\ m^{-3}$ HNO_3, 10 $\mu g\ m^{-3}$ H_2SO_4 and 0 $\mu g\ m^{-3}$ HCl. The relative humidity is 36% and the temperature 298 K. The mass below the solid line indicates the total amount of aerosol, with the incremental components of that total as indicated.

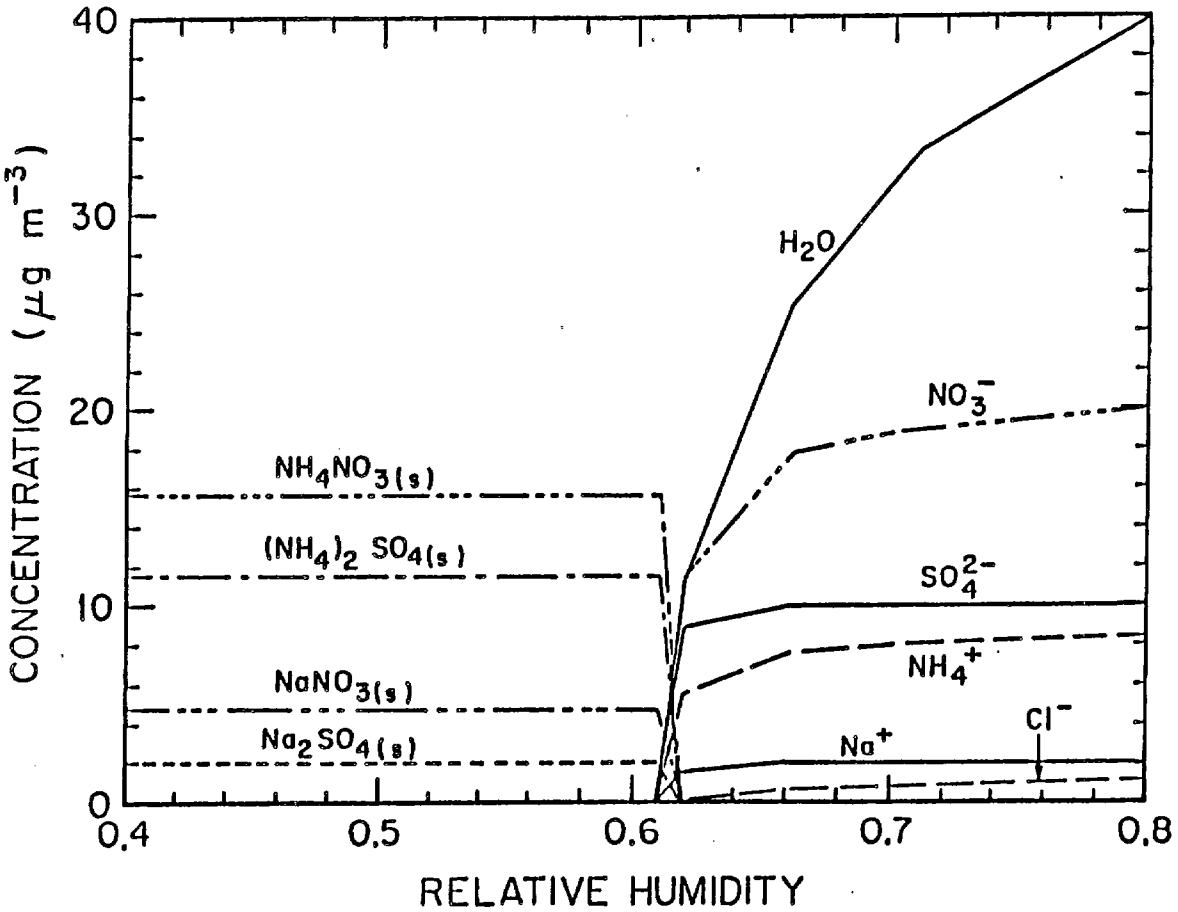

Fig. 7 Predicted aerosol composition as a function of the relative humidity for 10 μg m^{-3} NH_3. The other conditions are 5 μg m^{-3} NaCl, 20 μg m^{-3} HNO_3, 10 μg m^{-3} H_2SO_4 and 0 μg m^{-3} HCl, and the temperature is 298 K.

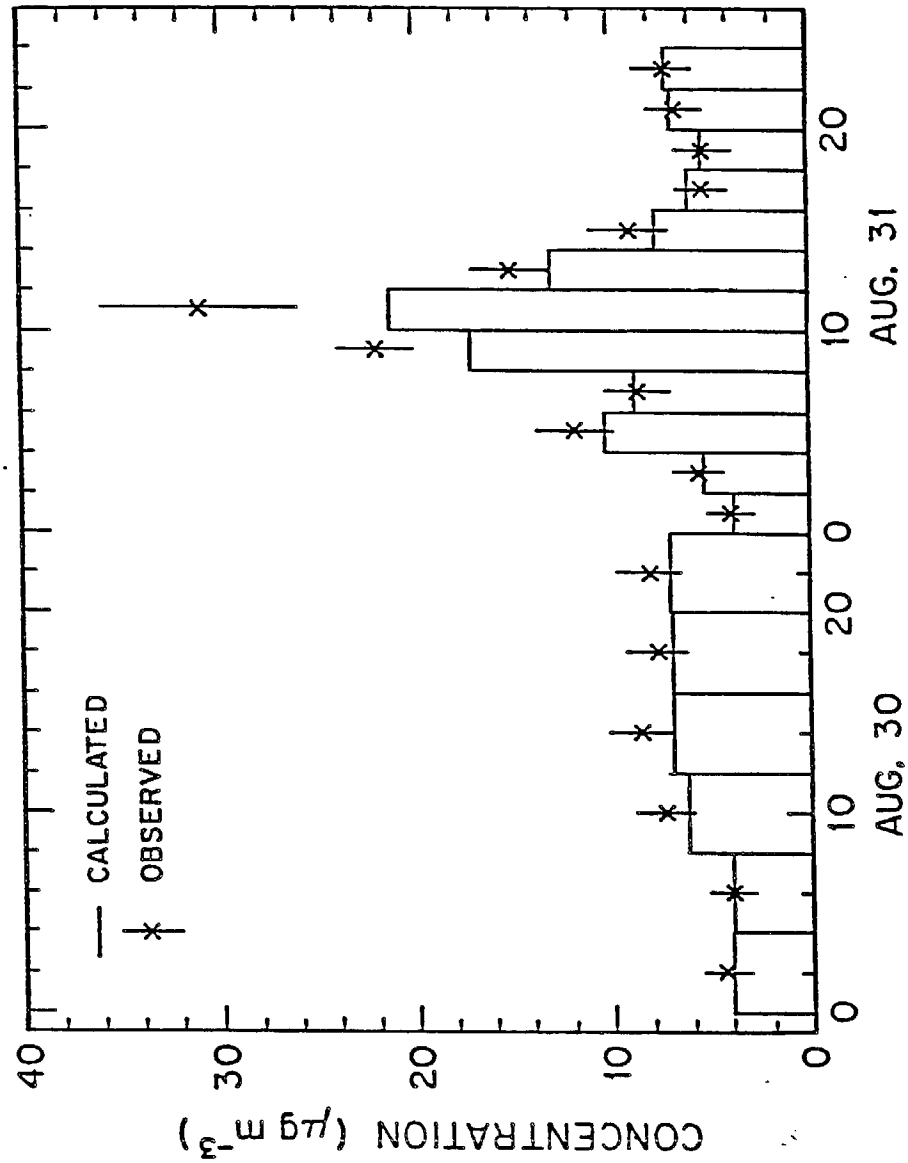

Fig. 8 Observed (Russell and Cass, 1984) and predicted nitrate concentrations at Long Beach, CA on August 30 and 31, 1982.

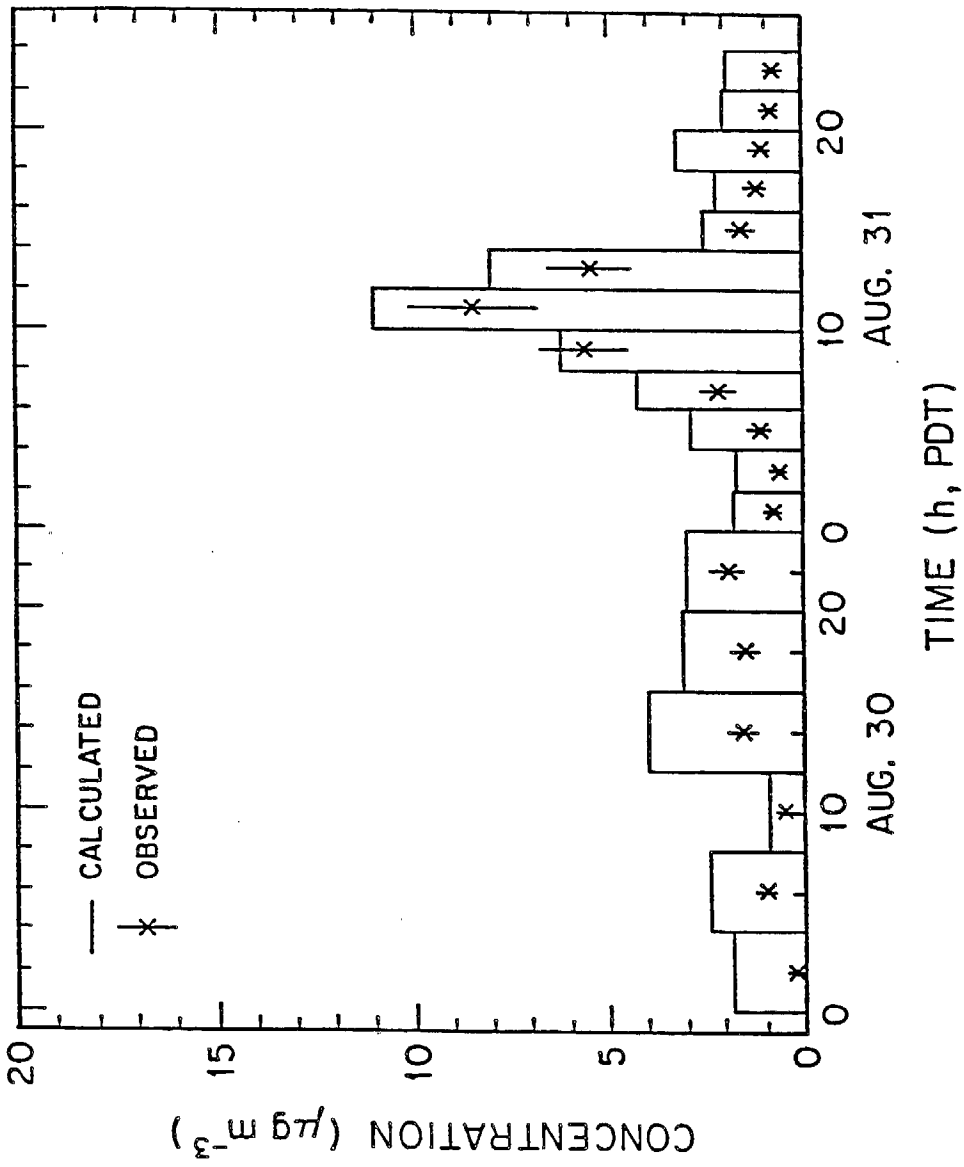

Fig. 9 Observed (Russell and Cass, 1984) and predicted ammonium concentrations at Long Beach, CA on August 30 and 31, 1982.

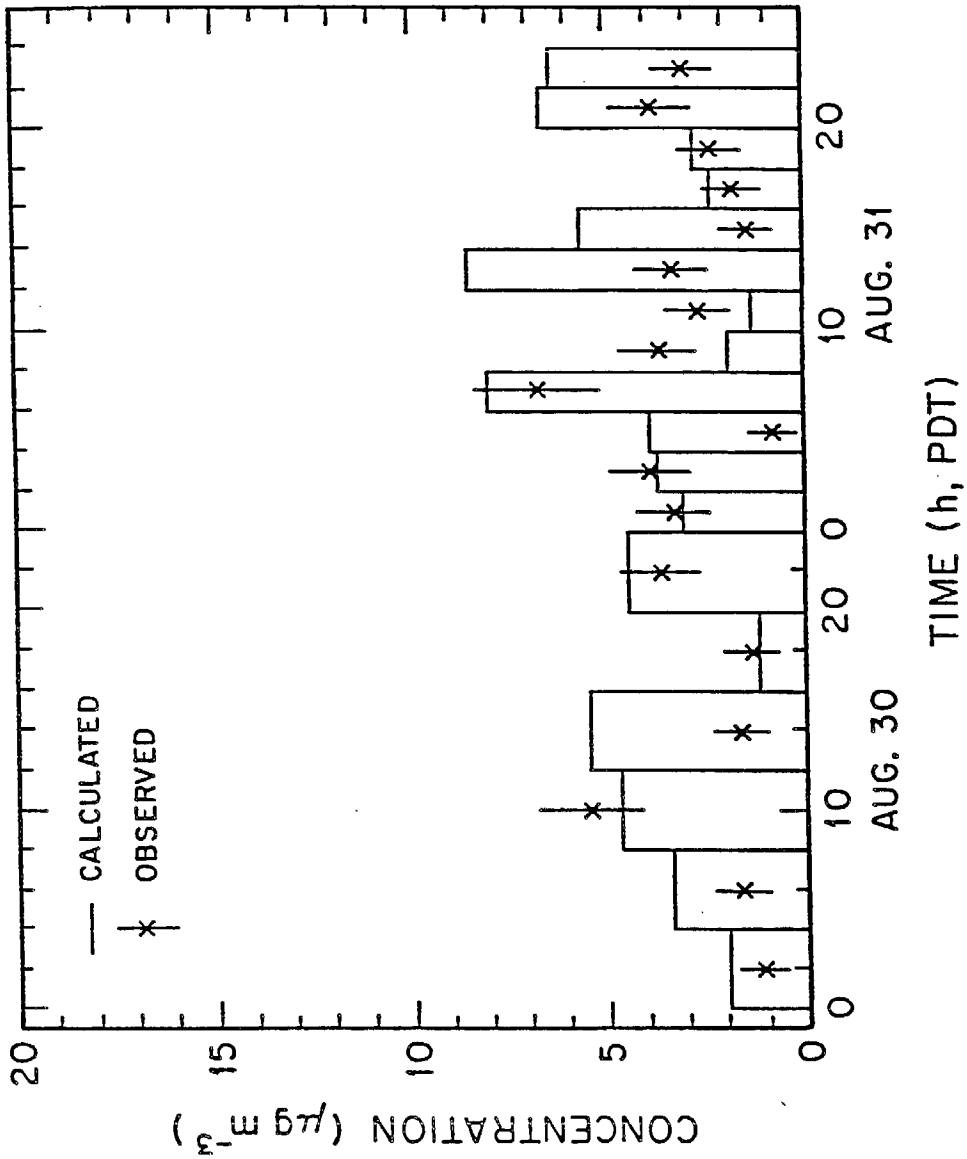

Fig. 10 Observed (Russell and Cass, 1984) and predicted chloride concentrations at Long Beach, CA on August 30 and 31, 1982.

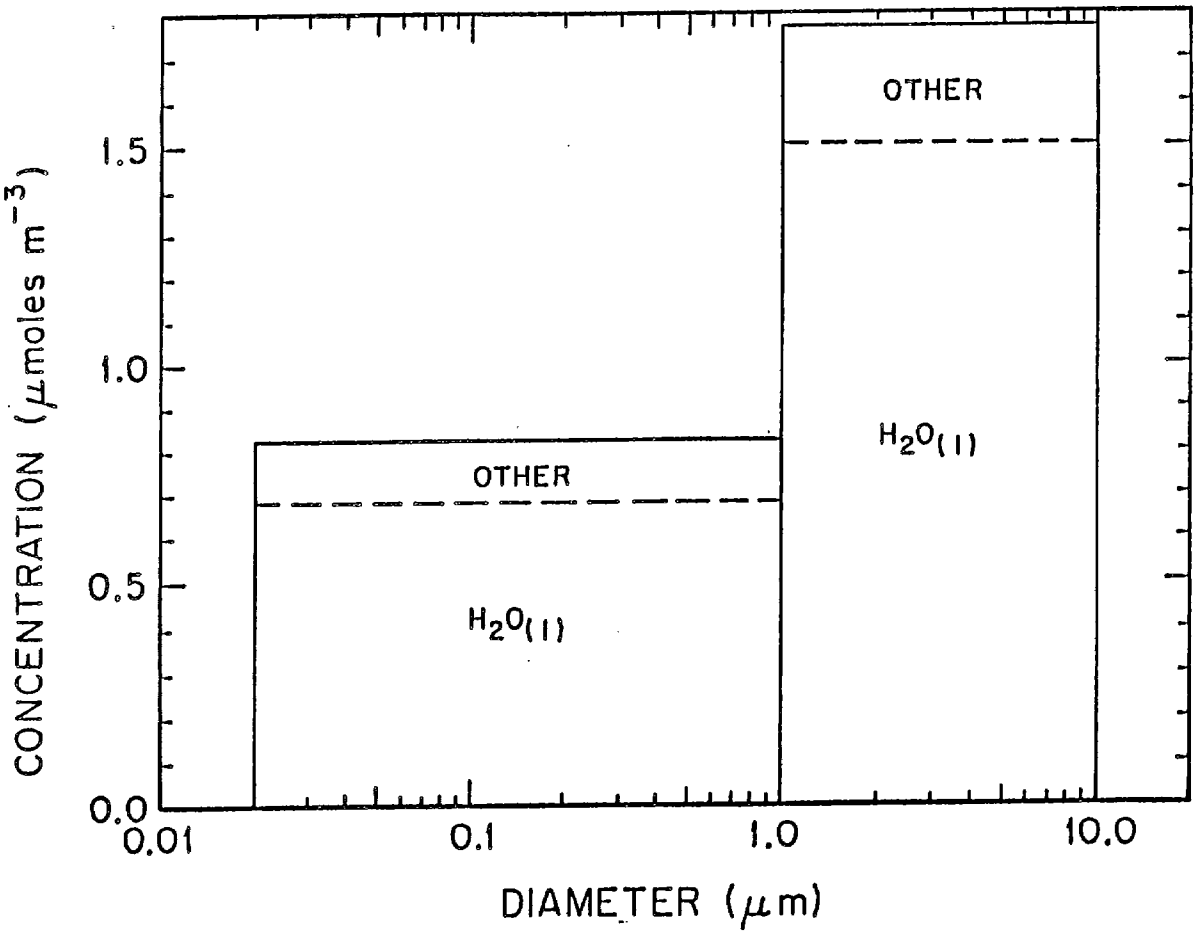

Fig. 11 Predicted size distribution of aerosol water at Long Beach, CA during the period 0000-0200 hours PDT on August 31, 1982. The relative humidity was 81%. The mass below the upper line indicates the total amount of aerosol, with the incremental components of that total as indicated.

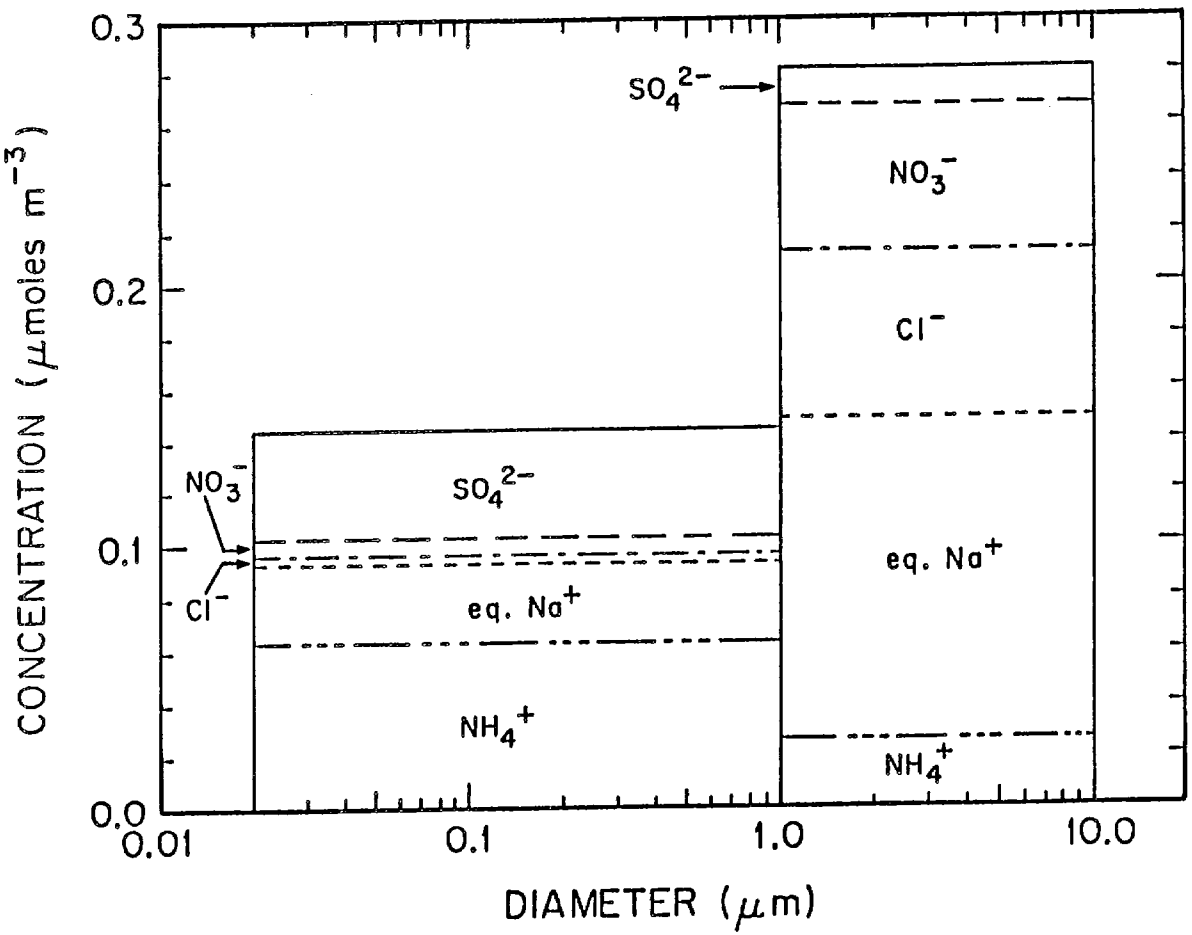

Fig. 12 Predicted size-composition distribution (exluding water) at Long Beach, CA during the period 0000-0200 hours PDT on August 31, 1982. The relative humidity was 81%. The mass below the upper line indicates the total amount of aerosol (exluding water), with the incremental components of that total as indicated.

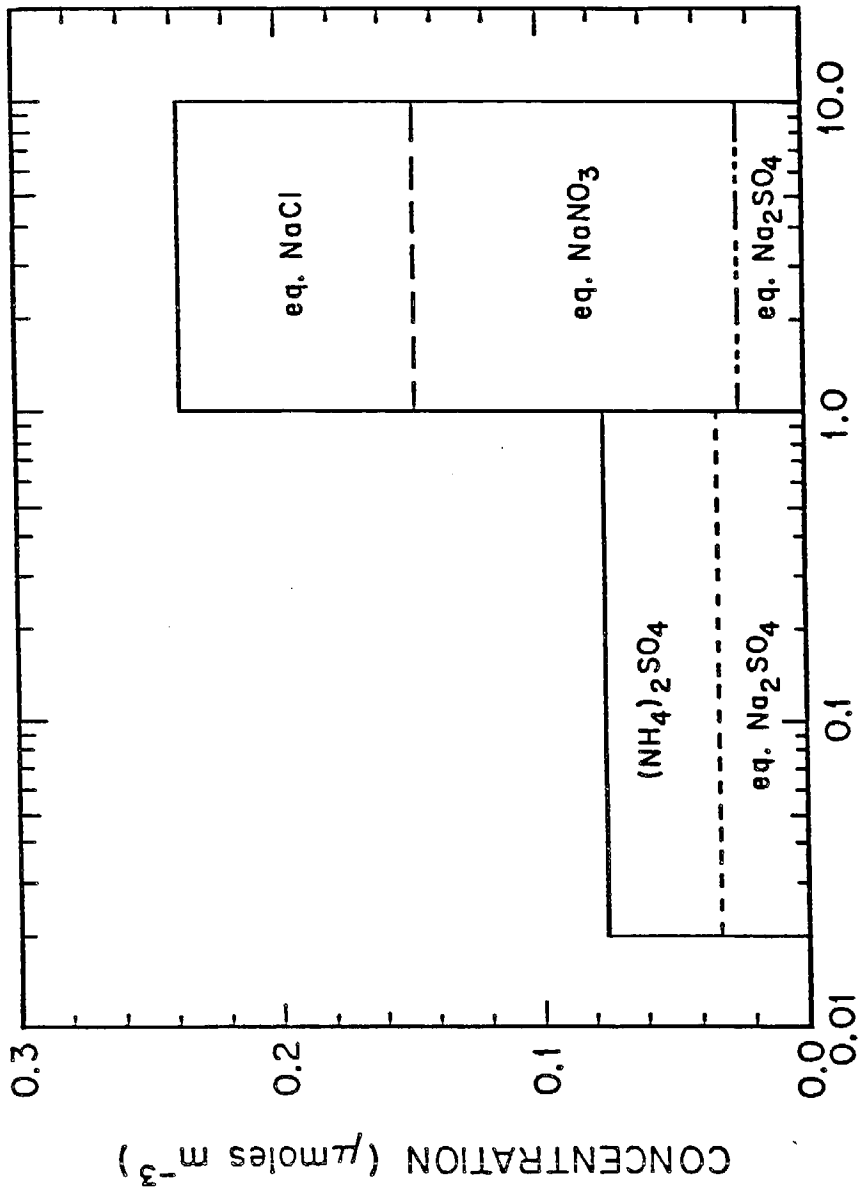

Fig. 13 Predicted size-composition distribution at Long Beach, CA during the period 1400-1600 hours PDT on August 31, 1982. The relative humidity was 43%. The mass below the upper line indicates the total amount of aerosol, with the incremental components of that total as indicated.

CHAPTER 4

ORGANIC AEROSOLS

ORGANIC AEROSOLS

Organic compounds are recognized as key ingredients of the polluted atmosphere and constitute a significant fraction of the urban aerosol. Organic aerosols reside primarily in the fine range of the particulate matter, thus contributing to the visibility degradation problem in the South Coast Air Basin (Gray, 1986). In general organic aerosols consist of both primary and secondary compounds. Primary organic species are emitted directly into the atmosphere as products of combustion processes (Gray, 1986). We have included primary organic aerosol emissions in our trajectory aerosol model. If the distribution of the emitted aerosol is known it can be very easily incorporated into the model, otherwise a default distribution, based on field studies (Wolff and Klimisch, 1982), is used.

Secondary organic species result from gas phase photochemical reactions involving hydrocarbons, ozone, nitrogen oxides and free radicals. In general the reactions of the various atmospheric hydrocarbons are of the form (Grosjean, 1976):

$$HC + X \longrightarrow I \longrightarrow \sum_i a_i P_i$$

where HC is the hydrocarbon, X is the oxidizing species, P_i is the i^{th} product resulting from reactions of the intermediate I, whose formation is the rate determining step, and a_i is the yield.

Among the possible reactants, X, only two are of major importance, ozone and the OH radical. Comparison of the reactivities of olefins and aromatics in their reactions with OH and O_3 shows that OH dominates in the oxidation of aromatics, whereas O_3 dominates in the oxidation of olefins (Grosjean, 1976).

The contribution of the various classes of hydrocarbons to the formation of particulate matter is a complex function of their relative ambient concentrations, gas-phase reactivity and ability to form products whose vapor pressure is low enough to produce aerosol.

Among the thousands of hydrocarbon species emitted in the atmosphere from combustion activities many do not generate condensible species, while others do produce condensible species but in negligible quantities. Table 1 summarizes aerosol yields measured during the photooxidation of various hydrocarbons. As shown in Table 1, paraffins, in general, even when irradiated at high concentrations, do not produce aerosol.

All unsaturated hydrocarbons are reactive with both O_3 and the hydroxyl radical, as well as NO_3. Not all of those, though, yield condensible products upon photooxidation. In general the reaction of olefins with O_3 and OH results in the formation of aldehydes, ketones and carboxylic acids (Niki et al, 1983) via the formation of the Crigee intermediate.

The straight chain olefins, reacting with O_3, produce species that have relatively high vapor pressures, and therefore do not produce aerosol. As the carbon number in the chain increases, the vapor pressure decreases. A sufficiently low vapor pressure for aerosol formation does not occur until the products have more than about ten carbons in their chain. Since straight chain olefins of such length exist in the atmosphere only in trace ammounts (Grosjean and Fung 1985), and since those smaller do not produce condensible species, we do not consider the straight chain olefins as organic aerosol precursors.

Cyclic olefins and diolefins have been found to produce aerosol upon photooxidation. Atmospheric oxidation of cycloalkenes has been recognized as a major source of difunctional compounds, which constitute a significant fraction of organic aerosol associated with photochemical smog (Hatakeyama et al; 1985, 1987). Among the various cycloalkenes, cyclopentene and cyclohexene are of major importance, because they are routinely found in gasoline and auto-exaust. Studies have been devoted to characterize the chemical identity of the condensible products of the photooxidation reactions of these two cycloalkenes (Hatakeyama et al, 1985, 1987; Izumi et al, 1987), and it has been reported that dicarboxylic acids, dialdehydes and oxo-carboxylic acids are the major products in the aerosol phase.

Dialdehydes are the major primary species produced from the cycloalkene-O_3 reactions, but they are subsequently oxidized to produce oxo-carboxylic acids, the further oxidation of which gives the dicarboxylic acids. The latter species have been reported to be the major constituents in the aerosol phase (Hatakeyma, 1985, 1987). As shown in Table 2, glutaric acid and adipic acid, the final products of the photooxidation of cyclopentene and cyclohexene, respectively, have sufficiently low vapor pressures to form aerosols. Thus it is reasonable to assume that these two dicarboxylic acids are the only aerosol products of the reactions of cyclopentene and cyclohexene with O_3 and use overall reactions for their production, in the form shown in Table 3.

Product characterization has been attempted by many investigators (O' Brien et al, 1975; Niki et al, 1983) for the reactions of diolefins with O_3. It has been reported that diolefins can form several types of Crigee intermediates and accompanying carbonyl products. The final products of the diolefin-O_3 reactions are dicarboxylic acids (Schwartz et al, 1974), which explains the observed high aerosol yields, as it is shown in Table 1. Three diolefins, 1,5-hexadiene, 1,6-heptadiene and 1,7-octadiene are included in the primary organic inventory of aerosol precursors. The overall reactions of the diolefins are shown in Table 3 and the physical properties of their condensible products are summarized in Table 2.

Another class of organics that gives aerosol products upon atmospheric photooxidation, as shown in Table 1, is aromatics. Aromatics currently comprise about 35% of the gasoline in the United States (Seinfeld et al, 1987) and are also used as industrial solvents. Among the various aromatics, toluene and the xylenes are of major importance, because they are present in substantial levels in the air of the South Coast Air Basin (Grosjean and Fung, 1984), and they are aerosol precursors.

In spite of numerous experimental studies, the detailed reaction pathways of aromatic

photooxidations are still not well understood (Atkinson et al, 1983; Gery et al, 1985, 1987). Rate constant considerations indicate that aromatics will react predominantly with OH. The OH-aromatic reaction proceeds via two pathways, H-atom abstruction and OH addition (Atkinson and Lloyd 1984; Gery et al, 1985). It has been reported (Gery et al, 1985, 1987) that the major pathway (87%) is the addition of OH onto the aromatic ring, producing cresols, while subsequent addition of NO_3 produces various nitrocresols and nitrotoluenes.

Three reactions involving aromatic hydrocarbons are included in the organic aerosol mechanism. Because of similarities in the reaction mechanisms and the rate constants o-,p-,m-xylenes were lumped together. The major products of the toluene-OH and xylene-OH reactions are cresols and dimethyl phenols. The molar yield of the cresol production from the first reaction is estimated to be about 24% of the reacted toluene, while the yield of the latter reaction is estimated to be about 17% of the reacted xylene (Gery et al, 1985, 1987). Once cresols and dimethylphenols are formed, through addition of NO_2 they form various nitrocresol and nitroxylene products (Gery et al, 1985, 1987; Seinfeld et al, 1987). It is estimated that the yield of the last reaction is about 30% of the cresols and the phenols reacted.

Physical properties of the various condensible species, produced by the aromatic photooxidation reactions are not known. For the purpose of our calculations the diffusion cofficient, the molecular weight and the solubility of the nitro-cresol were used, while saturation pressure data were taken from recent chamber experiments (Seinfeld et al, 1987).

In contrast to inorganic aerosols, organic aerosols, in spite of the fact that they have been found to constitute about 40% of the Los Angeles fine aerosol, have not been studied extensively. Thus no ambient data are available at this point, against which to compare our model. To demonstrate the capabilities of the model developed here, we have used hy-

pothetical concentrations for the organic aerosol precursors for the trajectory that started at about 1300 PDT on August 31, 1982 at Anaheim, California and terminated at about 1800 PDT of the same day at Rubidoux, California. We assumed for this run that the initial concentration of each of the five organic aerosol precursors included is equal to 0.1% the initial THC. Figure 1 shows the initial aerosol size-composition distribution, used in our calculation, based on thermodynamic equilibrium.

Figure 2 shows the predicted evolution of the aerosol concentration as a function of time. The first hour of the simulation (1300-1400 PDT), due to the intensive solar radiation, radicals, O_3 and hydrocarbons react and produce condensible species. These species, then, transfer to the particulate phase, totally via condensation onto preexisting particles, causing a rapid increase of the organic content of atmospheric aerosols during the first hour of the simulation. After 1400 PDT the increase of the concentration of the aerosol organics slows. This slowing is caused, primarily, by the conversion of much of the organic aerosol precursors during the intensive photooxidation activity of the first hour of the simulation. After 1600 PDT the organic aerosol concentration actually starts decreasing, mainly because deposition and aerosol transfer to the upper layers dominate over the organic aerosol production.

Figure 3 shows the predicted aerosol size composition distribution at Rubidoux. Comparison between Figures 1 and 3 shows that, when the parcel reaches Rubidoux the aerosol concentration is almost five times that at the beginning of the trajectory, at Anaheim.

REFERENCES

Atkinson, R., Carter, W. P. L., Darnall, R., Winer, A. M. and Pitts, J. N. (1980). A smog chamber and modeling study of the gas phase NO_x-Air photooxidation of toluene and cresols. Int. J. Chem. Kinet., 12, 779.

Atkinson, R. and Lloyd, A. C. J. Phy. Chem. Ref. Data, 13, 315 (1984).

Gery, M. W., Fox, D. L., Jeffies, H. E., Stockburger, L. and Weathers W. S. (1985). A continuous stirred tank reactor investigation of the gas phase reaction of hydroxyl radicals and toluene. Int. J. Chem. Kinet., 17, 931-955.

Gery, M. W., Fox, D. L., Kamens, R. M. and Stockburger, L. (1987). Investigation of hydroxyl radical reactions with o-xylene and m-xylene in a continuous stirred tank reactor. Environ. Sci. Technol. 21, 339-348.

Gray, H. A. (1986). Control of atmospheric fine primary carbon concentration. EQL Report No. 23.

Grosjean, D. (1976). Secondary organic aerosols and their gas phase hydrocarbon precursors. Symposium "Chemistry and Air pollutants, 1976".

Grosjean, D and Fung, K. (1984) Hydrocarbons and Carbonyls in Los Angeles Air. JAPCA 34:537-543

Grosjean, D. Ozone and other photochemical oxidants. National Academy of Sciences. National Research Council: Washington DC (1977)

Hatakeyama, S., Tanonaka, T., Weng, J., Bandow, H., Takagi, H. and Akimoto, H. (1985). Ozone-cyclohexene reaction in air: Quantitative analysis of particulate products and reaction mechanism. Environ. Sci. Technol. 19, 935-942.

Hatakeyama, S., Ohno, M., Weng, J., Takagi, H. and Akimoto, H. (1987). Mechanism for the formation of gaseous and particulate products from ozone-cycloalkene reaction in air. Environ. Sci. Technol. 21, 52-57.

Izumi, K., Murano, K., Mizuochi, M. and Fukuyama, T. (1987) Aerosol formation by the photooxidation of cyclohexene in the presence of nitrogen oxides. (Submitted for publication).

Leone, J. A., Flagan, R. C., Grosjean D. and Seinfeld, J. H. Int. J. Chem. Kinet., 17,

177 (1985).

Niki, H., Maker, P., Savage, C. M. and Breitenbach, L. P. (1983). Atmospheric ozone-olefin reaction. Environ. Sci. Technol. 17, 312A-322A.

O' Brien, R. J., Holmes, J. R. and Bockian, A. H. (1975). Formation of photochemical aerosol from hydrocarbons. Chemical reactivity and products. Environ. Sci. Technol. 9, 568-576.

Schwartz, W. (1974). Chemical characterization of model aerosols. EPA-650/3-74-011. Columbus Ohio: Battelle Memorial Insitute.

Seinfeld, J. H., Flagan, R. C., Petti, T. B., Stern, J. E. and Grosjean, D. (1987). Aerosol formation in aromatic/NO_x systems. CRC project No. AP-6 Final Report.

Uno, I., Wakamatsu, S., Wadden, R. A., Konino, S., and Koshio, H. (1985). Evaluation of hydrocarbon reacivity in urban air. Atmospheric Environment 19, 1283-1293.

Wolff, G. T. and Klimisch R. L. (1982). Particulate Carbon. Atmospheric Life Cycle. Plenum Press, New York, page 297.

Table 1: Aerosol yields from various organics

SPECIES	ELECTROPHILE	MOLAR YIELD (%)[a]	REFERENCE
PARAFFINS			
n-heptane	OH, O_3	0.06	NAS 1977
2,6 dimethylheptane	OH, O_3	0.1	NAS 1977
2,4,4 trimethylpentane	OH, O_3	0.7	NAS 1977
cyclopentane	OH, O_3	0.0	NAS 1977
cyclohexane	OH, O_3	0.17	NAS 1977
OLEFINS			
2 methyl 1 butene	OH, O_3	0.0	NAS 1977
2 methyl 2 butene	OH, O_3	0.0	NAS 1977
3 methyl 1 butene	OH, O_3	0.0	NAS 1977
2 pentene	OH, O_3	0.0	NAS 1977
3 hexene	OH, O_3	0.0	NAS 1977

Table 1: Continued

SPECIES	ELECTROPHILE	MOLAR YIELD (%)[a]	REFERENCE
cyclopentene	O_3	39	Grosjean and Friedlander 1980
cyclohexene	O_3	15	Hatakeyama et al 1985
1,5 hexadiene	O_3	11	NAS 1977
1,6 heptadiene	O_3	19	NAS 1977
1,7 octadiene	O_3	15	NAS 1977
AROMATICS			
toluene	OH	2	Stern et al 1987
xylene	OH	1.5	Stern et al 1987

a) Molar yields have been obtained from carbon mass yields by assuming that the only species in the aerosol phase are those shown in Table 3.

Table 2: Physical properties of condensible organics.

Species	MW	D ($m^2 sec^{-1}$)	p (Pa)	Solubility(kg/kg-H_2O)
succinic acid	118	8.22×10^{-6}	3.96×10^{-5}	8.30×10^{-2}
glutaric acid	132	7.51×10^{-6}	1.80×10^{-5}	1.30
adipic acid	146	6.96×10^{-6}	8.19×10^{-6}	3.00×10^{-2}
nitro-cresol	153	7.13×10^{-6}	8.00×10^{-6}	3.40×10^{-11}

Table 3: Organic aerosol-producing reactions

Reaction	Rate Constant ($ppm^{-1}\ min^{-1}$)
$CH_2 = CH - (CH_2)_2 - CH = CH_2 \xrightarrow{O_3} 0.11 \quad HCOO - (CH_2)_2 - COOH$	8.26×10^{-2}
$CH_2 = CH - (CH_2)_3 - CH = CH_2 \xrightarrow{O_3} 0.19 \quad HCOO - (CH_2)_3 - COOH$	5.25×10^{-2}
$CH_2 = CH - (CH_2)_4 - CH = CH_2 \xrightarrow{O_3} 0.15 \quad HCOO - (CH_2)_4 - COOH$	3.35×10^{-2}
cyclopentene $\xrightarrow{O_3} 0.39 \quad HCOO - (CH_2)_3 - COOH$	1.56
cyclohexene $\xrightarrow{O_3} 0.15 \quad HCOO - (CH_2)_4 - COOH$	0.328
toluene $\xrightarrow{OH} 0.24 \quad$ cresol	9.10×10^3
xylene $\xrightarrow{OH} 0.17 \quad$ dimethyl – phenol	2.65×10^4
cresol or dimethyl – phenol $\xrightarrow{NO_3} 0.30 \quad$ nitro – cresol	2.20×10^4

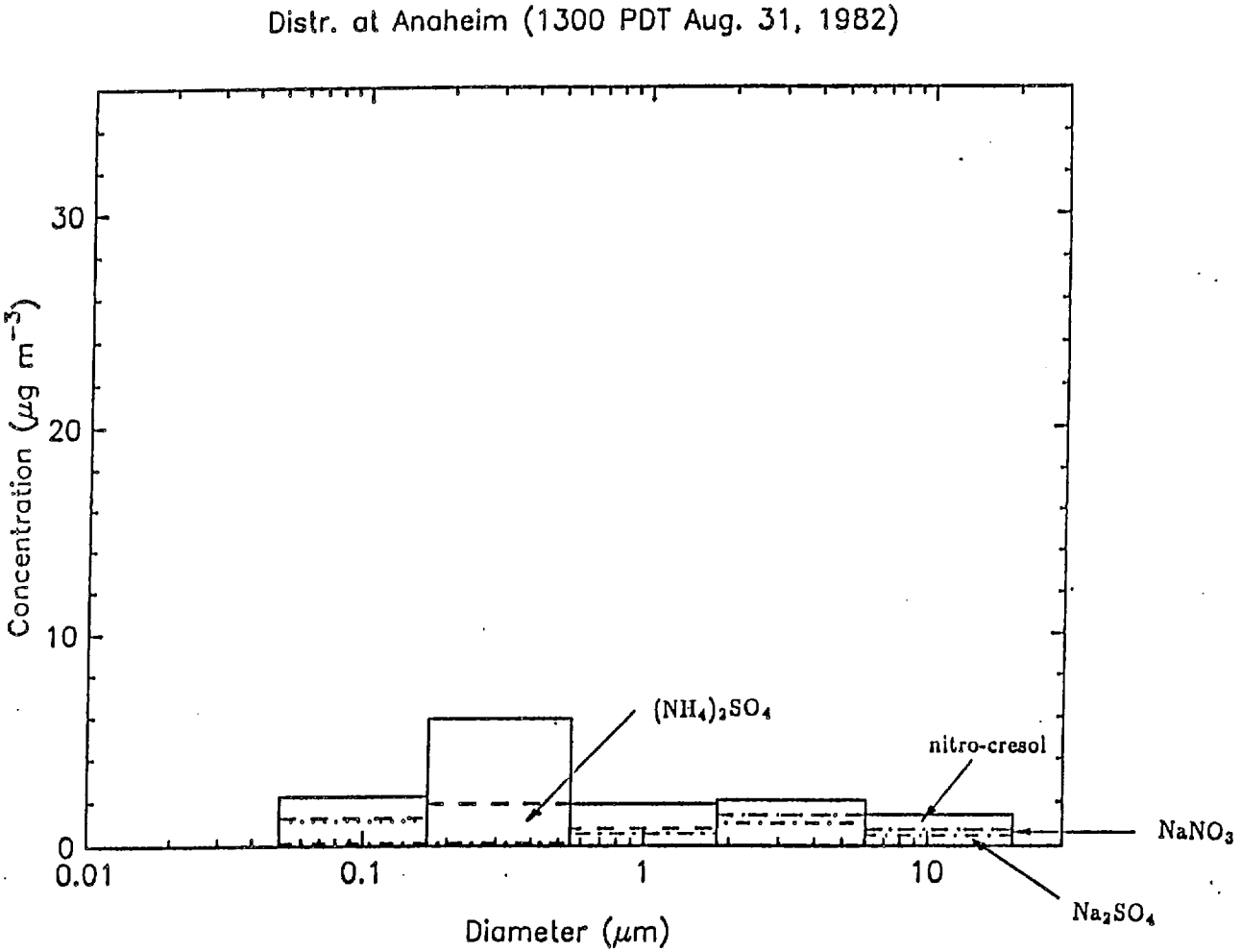

Fig. 1 Calculated aerosol size-composition distribution at Anaheim, CA at 1300 hours on August 31, 1982. The mass below the solid line indicates the total amount of aerosol, and the incremental components of that total are indicated.

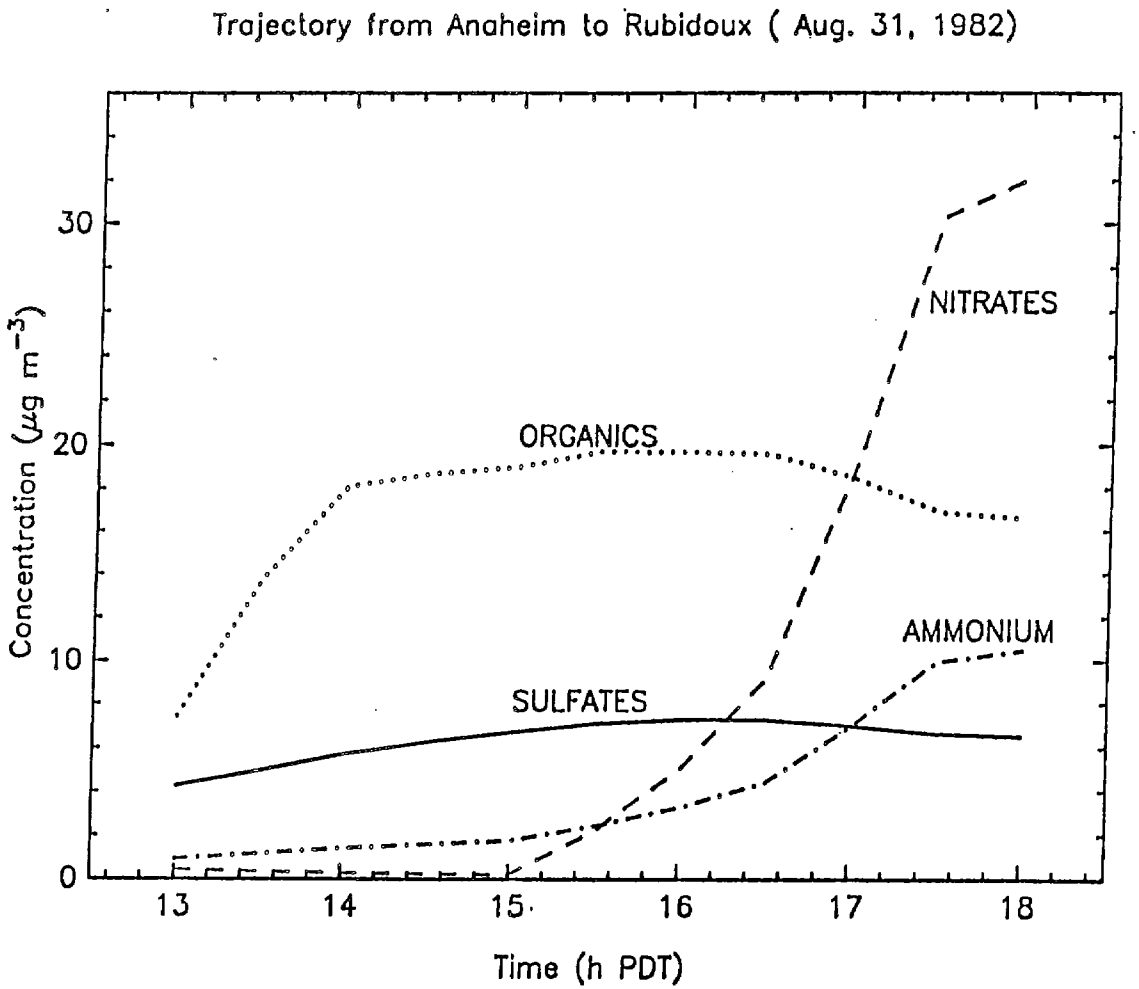

Fig. 2 Predicted evolution of total aerosol nitrate, ammonium, sulfate and organics along the trajectory from Anaheim to Rubidoux, CA from 1300 to 1800 hours on August 31, 1982.

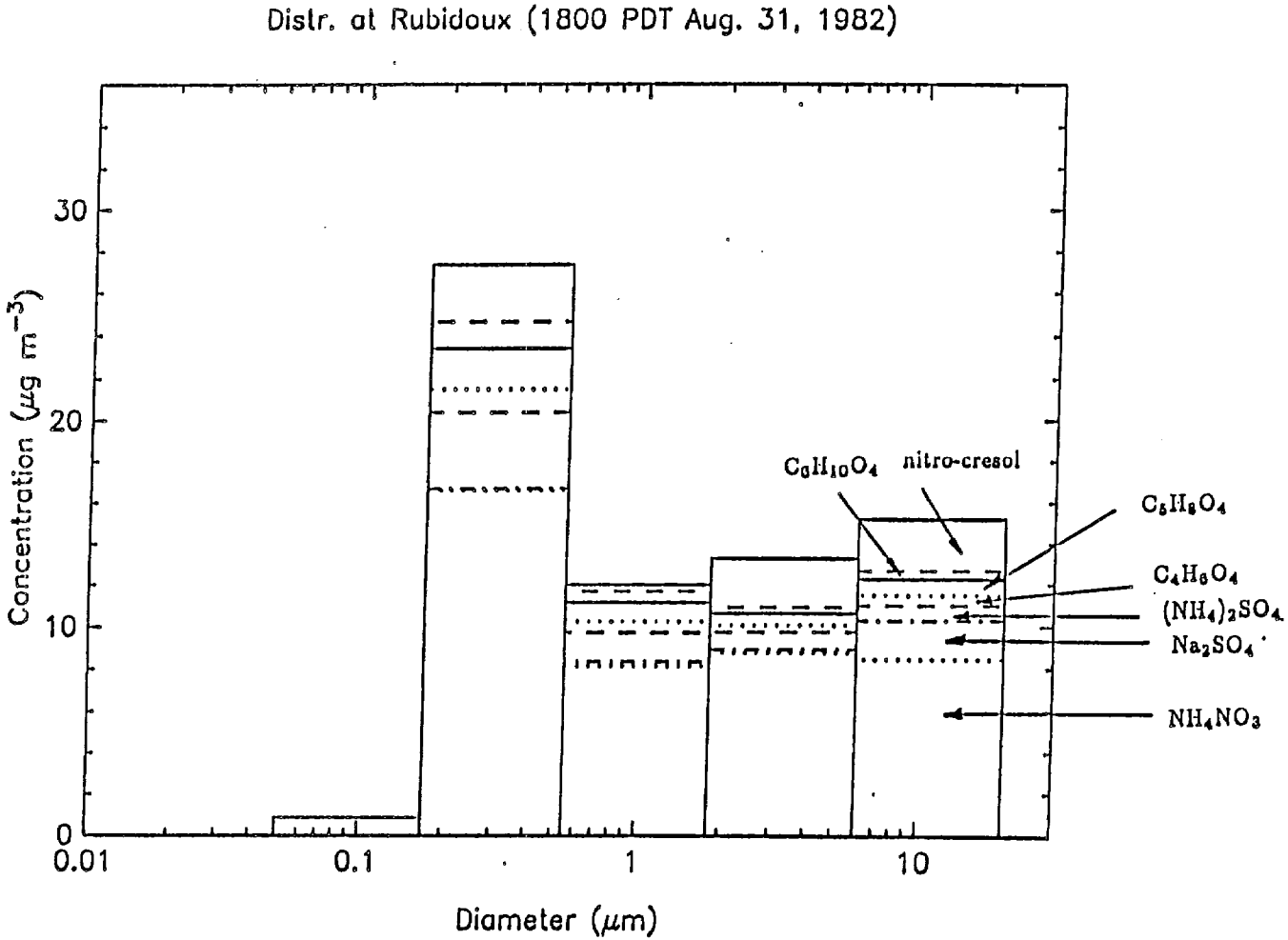

Fig. 3 Predicted size-composition distribution at Rubidoux, CA at 1800 hours on August 31, 1982. The mass below the solid line indicates the total amount of aerosol, and the incremental components of that total are indicated.